

*Feature Article***The Science of Digitizing Paintings for Color-Accurate Image Archives: A Review****Roy S. Berns^{▲*}***National Gallery of Art, Washington, DC*

A review of the human visual system, the CIE L*, a*, b* color space and its use in evaluating color image quality, and digital image capture is presented, the goal of which is to provide background information for imaging professionals involved in creating digital image databases for museums, galleries, archives, and libraries. Following this review, an analysis was performed to determine the effects of bit depth, dynamic range, gamma correction, and color correction on the ability to estimate colorimetric data from R, G, B digital images with a minimum of error. The proper use of gray scale and color targets was also considered. Recommendations are presented for the direct digital image capture of paintings. Finally, a brief look into the future using spectral imaging techniques is presented.

Journal of Imaging Science and Technology 45: 305–325 (2001)

Introduction

Digital image databases have become ubiquitous with museums, galleries, archives, and libraries. (For simplicity, “museum” will be used to represent the many repositories.) Connect to their websites and a wealth of visual information is available. Museums are sharing their images to increase access such as the Art Museum Image Consortium, AMICO, a subscription program for educational institutions (see www.amico.org). The quality of the digital images can be quite varied. Leaving aside the issue of the long-term storage of digital information, clearly a critical issue but beyond the scope of this publication, there are many reasons that quality might be poor. Some are philosophical in origin where there is a deliberate decision not to create a high-quality accurate representation, rather, a database of low-quality “thumbnail” images. Some reasons are technical in origin; and some are caused by constraints imposed by the sheer magnitude of creating and maintaining a digital archive of many thousands, and in some cases, hundreds of thousands of images. Finally, images available to the public through the internet are usually of low resolution as well as designed for CRT display. These are “derivative” images created from the “master” image. A digital master is a result of direct digital capture of the work of art.

The technical problems are manifest almost immediately. Trying to define specifications for image capture,

storage, retrieval, and display (both in soft and printed forms) with an eye on cost, time, and who will do the work is extremely challenging.^{1–3} Because the scope of this publication is limited to direct digital capture of paintings and will not address digitizing photographic collections or photographic reproductions of paintings, conservation issues are especially important. The process of digitizing must not damage the painting, which could occur all too easily by excessive handling and irradiation by high-intensity light sources. Blackwell⁴ and Lossau and Liebetru⁵ have considered these issues in practice. Clearly, it is desirable to digitize the art once and in a manner that facilitates a variety of derivatives created for a variety of applications, be it web-based, printed publication, scientific analysis, or any number of scholarly endeavors by art historians.

Thus the purpose of this publication is to provide sufficient background to aid in setting specifications for color image-capture systems. Having presented this background, it is possible to propose a methodology for digital image capture that minimizes the inherent limitations of many digital systems in use today. Finally, considerations will be given to the future. What are the optimal characteristics of a digital imaging system designed to record paintings?

**A Review of Digital Imaging
The Human-Visual System**

The first step in understanding digital imaging is to understand about the human visual system. Four concepts will be defined: spectral sensitivity, opponent encoding, spatial resolution, and nonlinear response. This description is very simplified. For greater detail, but still at a qualitative level, see Berns.⁶ For a thorough understanding of the human visual system, see Wandell⁷ and Kaiser and Boynton.⁸

Incident light interacts with visual receptors, rods and cones. Following a chemical reaction, light energy is con-

Original manuscript received June 5, 2000

▲ IS&T Member

* Permanent address: Munsell Color Science Laboratory, Chester F. Carlson Center for Imaging Science, Rochester Institute of Technology, Rochester, New York; berns@cis.rit.edu

Supplemental Materials—Web Figures 1 through 3 can be found in color on the IS&T website (www.imaging.org) for a period of no less than 2 years from the date of publication.

©2001, IS&T—The Society for Imaging Science and Technology

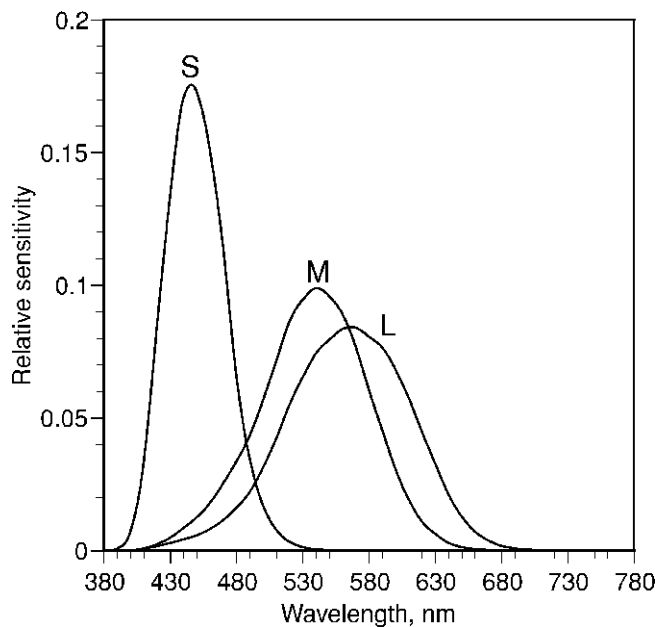


Figure 1. The spectral sensitivities of the human-visual system's cone⁹ (normalized to equal area).

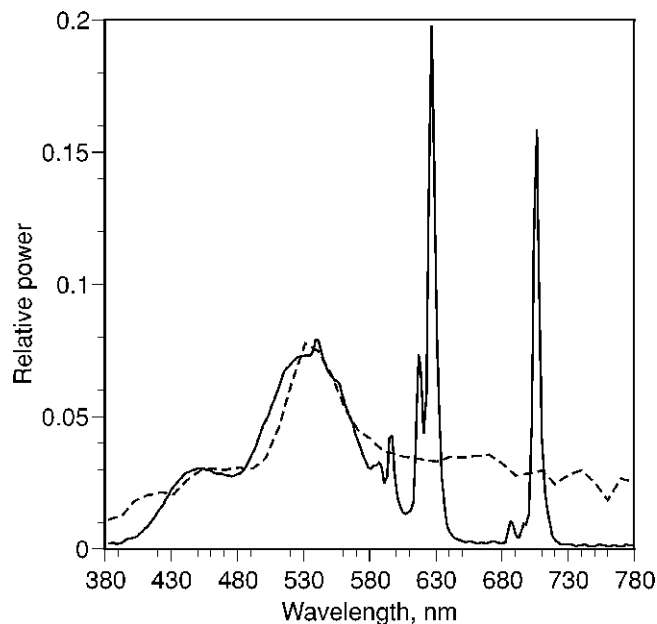


Figure 2. Spectral properties of a metamer pair formed by foliage, illuminated by natural daylight (dashed line), and a CRT display (solid line).⁶

verted to a neural signal. There are three classes of cones (our color receptors), L, M, and S, named for their dominant sensitivity to long, medium, and short wavelengths of light. Each has a unique spectral sensitivity, shown in Fig. 1. Spectral sensitivity defines a detector's sensitivity as a function of wavelength. Because there are only three types of cones and their spectral sensitivities are broad, many different objects can produce the same cone responses, leading to the identical color. This is known as metamerism (pronounced "me-tam'er-ism") and explains why color reproduction is possible in which small numbers of colorants can reproduce our world, composed of thousands of colorants. A metameric match between foliage, illuminated by natural daylight, and a CRT color reproduction of the foliage is shown in Fig. 2. Despite large differences in their spectral properties, these two stimuli match in color.

The cones combine spatially and form opponent signals, white/black, red/green, and yellow/blue. During the late 1800's, Hering considered these six colors as elemental, shown in Fig. 3. Lines connecting the various elemental colors indicate possible continuous perceptions. There are not lines connecting yellow and blue and red and green. It is not possible to have a color that is simultaneously reddish and greenish, for example.

Because there are different numbers of each cone type, when they combine to form opponent signals, there are different spatial resolutions among the opponent signals. Spatial resolution defines the resolving power of an imaging system and leads to the ability to discern fine detail. The black/white signal has the highest spatial resolution, followed by the red/green signal. The yellow/blue signal has quite low spatial resolution. These differences in spatial resolution have been exploited in image compression such as JPEG.¹⁰ The concept of "visually lossless compression" originates with this property of the eye. Spatial resolution is reduced in the chromatic channels in a manner that results in images that look identical to their uncompressed counterparts when viewed at typical distances, hence the term "visually lossless." However, information is still being discarded.

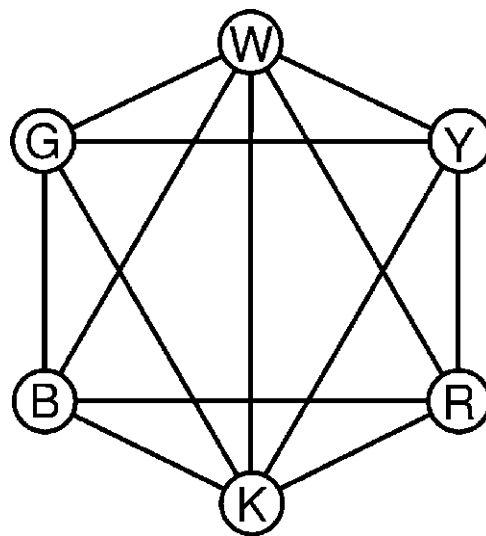


Figure 3. Six elemental colors postulated by Hering along with lines indicating possible perceptions, e.g., yellowish red (W = white; Y = yellow; R = red; K = black; B = blue; G = green) .

The neural processing from cone-receptor signals through signals interpreted by the brain and resulting in color names such as yellow, brown, and gray is exceedingly complex. Every year, vision scientists fill in more pieces of the puzzle. From a practical perspective, it is very useful to have a simple mathematical model that enables color perceptions to be estimated from light imaged onto our visual system. A model was derived by the International Commission on Illumination (CIE) in 1976, known as CIE L^* , a^* , b^* (pronounced "el-star" and so on) or its official abbreviation, CIELAB (pronounced "see-lab").¹¹ The coordinates, L^* , a^* , and b^* represent the perceptions of lightness, redness/greenness, and yellowness/blueness, respectively.

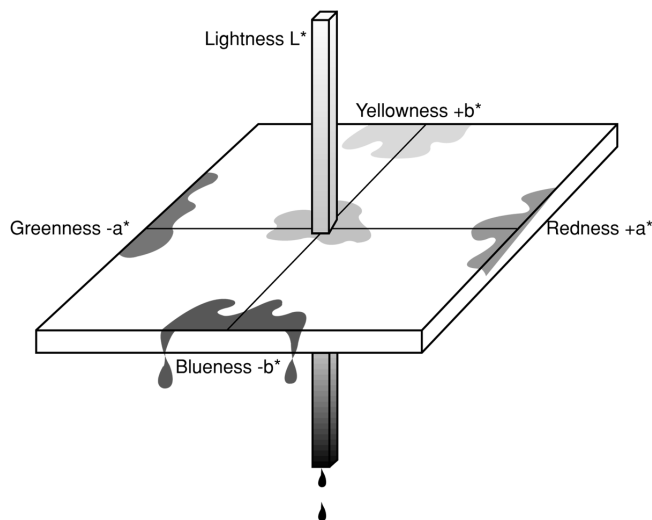


Figure 4. Conceptualized CIELAB color space.⁶

CIELAB is considered a color space in which positions indicate an object's color. This type of color space is diagrammed in Fig. 4. The coordinates are calculated from the knowledge of an object's spectral reflectance or transmittance properties, a light source interacting with the object, and the spectral sensitivities of an observer. For a number of reasons, the L, M, and S spectral sensitivities, shown in Fig. 1, are not used; rather, a set of curves mathematically related to spectral sensitivities, known as color-matching functions,^{6,11} are used instead.

The complex signal processing of the visual system results in a nonlinear (curved) relationship between light imaged onto the eye and color perceptions, shown in Fig. 5 for lightness. This means that for dark colors, small changes in an object's reflectance or transmittance lead to large changes in lightness. For light colors, the opposite occurs: Large changes in an object's reflectance or transmittance lead to small changes in lightness. This curvature is known as a compressive function. This compression also occurs for the chromatic channels.

In summary, the human visual system has three cone types, each with unique spectral sensitivities that overlap greatly. They combine spatially forming opponent signals: white/black, red/green, and yellow/blue. Each channel has a different spatial resolution. The relationship between incident light and color perceptions is nonlinear. A simple model, CIELAB, can be used to calculate color perceptions from measurements of the object, its illumination, and the observer.

The Digital Camera

Digital cameras consist of three main components: input optics, sensor, and signal processing. The optical system is typical of conventional photography in which a scene is imaged on to a two-dimensional plane, much like the human visual system.¹² Light interacts with a sensor, often a charged-couple device (CCD) that converts light energy to an electrical signal.¹³ The sensor may be one-dimensional—a single row of sensors—or two-dimensional—a grid of sensors. In one-dimensional systems, the row of sensors is scanned across the image plane. These are "scanbacks" and are similar to flat-bed scanners. Because scanning occurs, the objects be-

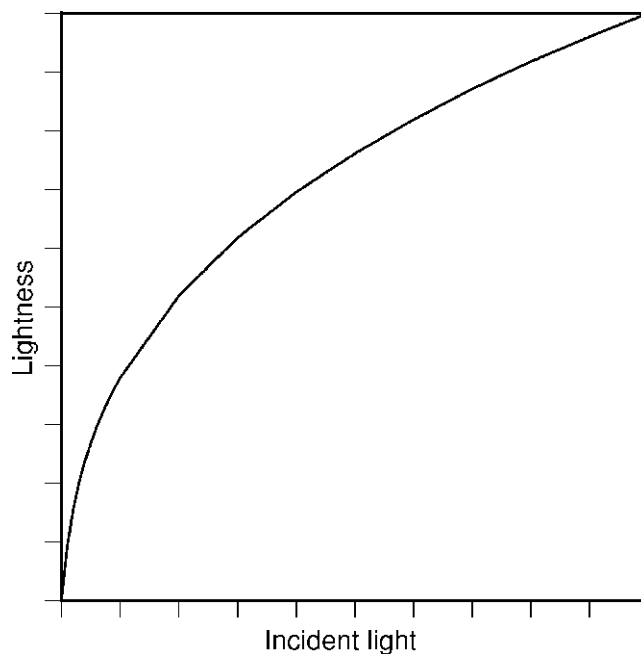


Figure 5. Nonlinear response between incident light and lightness. The incident light can have units of radiance, irradiance, luminance, illuminance, or simply power per unit area. (CIE L^* is used as a representation of lightness.)

ing digitized are stationary. Through signal processing, the electrical signal is converted to a digital signal.

For color, the one-dimensional detector array is trebled, each array having either a red, green, or blue filter in front of the detector, often referred to as "trilinear arrays." In some systems, a color filter wheel is positioned between the optical system and a monochrome, i.e., grayscale, scanning array. The array scans across the image plane multiple times, once for each filter-wheel position. For two-dimensional arrays, detectors are filtered in a mosaic pattern. Similar to the human visual system, there is not the same number of red, green, and blue sensors. Image processing is used to interpolate missing data for each color plane, sometimes called "demosaicing." The design of the mosaic and accompanying image processing is optimized to minimize artifacts caused by sampling, known as "aliasing." It is also possible to have three two-dimensional monochrome arrays, each filtered with either a red, green, or blue filter or a single two-dimensional array and filter wheel. These systems do not require the complex interpolation procedures.

For color accuracy, the most important characteristic of the digital camera is its spectral sensitivities. Ideally, they should closely resemble the human visual system's spectral sensitivities shown in Fig. 1. Strictly, a camera's spectral sensitivities should be a linear transformation of the human visual system's spectral sensitivities.¹⁴ That is, through a linear transformation, the L, M, and S sensitivities are well estimated. Thus, CIE color-matching functions, which do not resemble L, M, and S sensitivities, meet this criterion. This is also known as the Luther or Luther-Ives condition. For many scanbacks, this critical characteristic is seldom achieved, shown in Fig. 6. It is seen that these sensitivities have very little overlap and the position of the red sensitivity is shifted considerably to longer wavelengths. It is

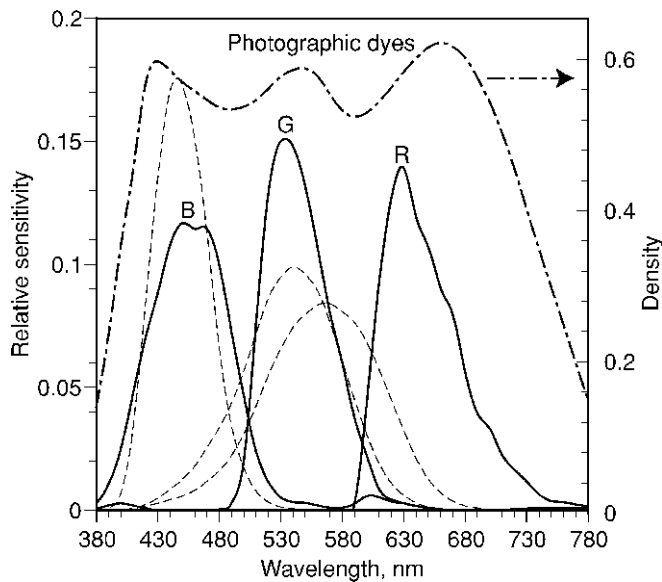


Figure 6. Spectral sensitivities of a typical scanback (solid lines), normalized to equal area. These sensitivities include the CCD spectral sensitivity, filter transmittances, and infrared radiation blocking filter. The human visual system's spectral sensitivities, shown in Fig. 1, are also plotted (dashed lines) as is the spectral density of typical photographic dyes combined to reproduce a medium-gray color (dashed-dotted line).

important to note that these sensors were designed for flat-bed scanners. These devices are optimized for imaging photographic materials. These sensitivities are “densitometric,” rather than “colorimetric.” They are designed to record the amounts, i.e., densities, of cyan, magenta, and yellow dyes in color photographic materials.¹⁵ Also shown in Fig. 6 is the spectral density, calculated by $D\lambda = -\text{Log}_{10}(R\lambda_{\text{gray}}/R\lambda_{\text{paper}})$, of color-paper photographic dyes reproducing a medium gray color. The blue and green peak sensitivities of the scanback are approximately coincident with the yellow and magenta dye peaks. The red sensitivity is not coincident to the cyan dye, but shifted to shorter wavelengths. This is a result of the particular IR cut-off filter used in this camera system, selected to improve its colorimetric performance when used as a scanback. When the sensor is used in a scanner, a different IR cut-off filter would be used. If a photographic collection were digitized using this type of scanback, it is possible to transform the R, G, and B data to highly accurate L^* , a^* , b^* estimates, though the computations are complex and for some photographic materials, the spectral sensitivities would need to be changed.¹⁶⁻¹⁸ When digitizing paintings, densitometric spectral sensitivities will result in large errors, even with the addition of color management, demonstrated in a latter section. Unfortunately, these types of digital cameras are the most common types used to create digital archives.⁴

Figure 7 is a plot of the spectral sensitivities of typical digital cameras employing color CCD two-dimensional arrays. There is considerably more overlap than densitometric scanbacks. However, the red sensitivity is still shifted towards longer wavelengths. It must be noted that color accuracy is only one of a number of criteria when designing a digital camera. Low-light sensitivity, image noise, resolution, read-out speed, manufacturing costs, and so on all must be considered.

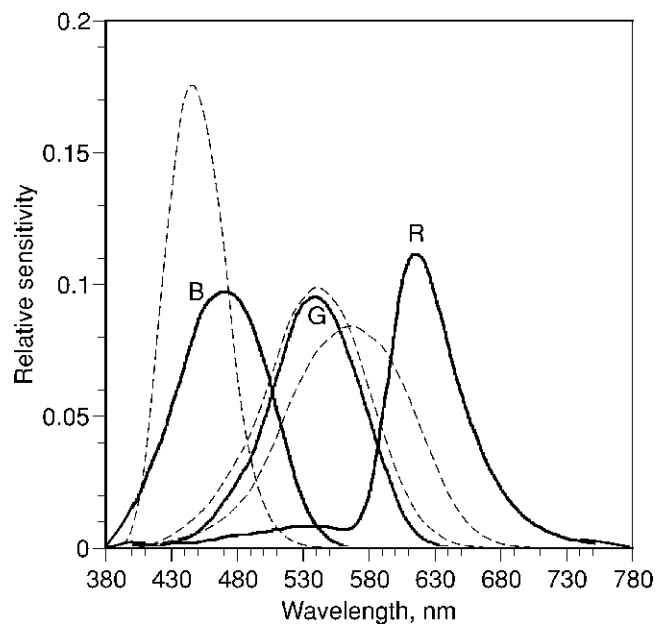


Figure 7. Spectral sensitivities of a typical color CCD two-dimensional array (solid lines), normalized to equal area. These sensitivities include the CCD spectral sensitivity, filter transmittances, and infrared radiation blocking filter. The human visual system's spectral sensitivities, shown in Fig. 1, are also plotted (dashed lines).

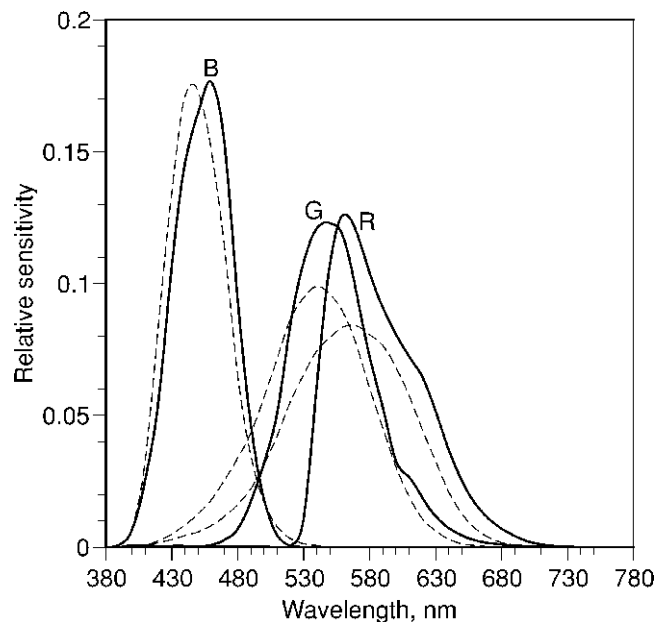


Figure 8. Spectral sensitivities of a monochrome scanback with three optimized color filters (solid lines), normalized to equal area. These sensitivities include the CCD spectral sensitivity, filter transmittances, and infrared radiation blocking filter. The human visual system's spectral sensitivities, shown in Fig. 1, are also plotted (dashed lines).

Many of these design criteria are mutually exclusive; the final design is always a compromise.

Figure 8 is a plot of the spectral sensitivities of a monochrome scanner with a filter wheel. The key design criterion was color accuracy. The spectral sensitivities of this camera system are much closer to the human vi-

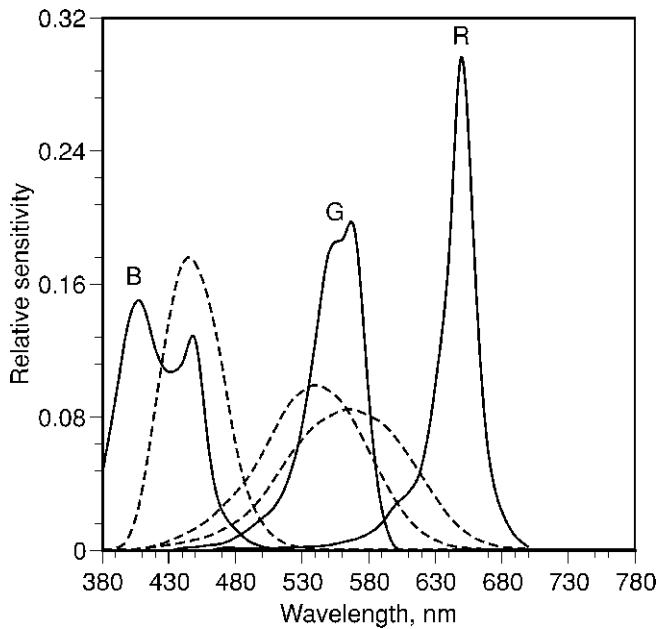


Figure 9. Spectral sensitivities of typical transparency film (solid lines), in this case Eastman Kodak Ektachrome 64T.¹⁵ The human visual system's spectral sensitivities, shown in Fig. 1, are also plotted (dashed lines).

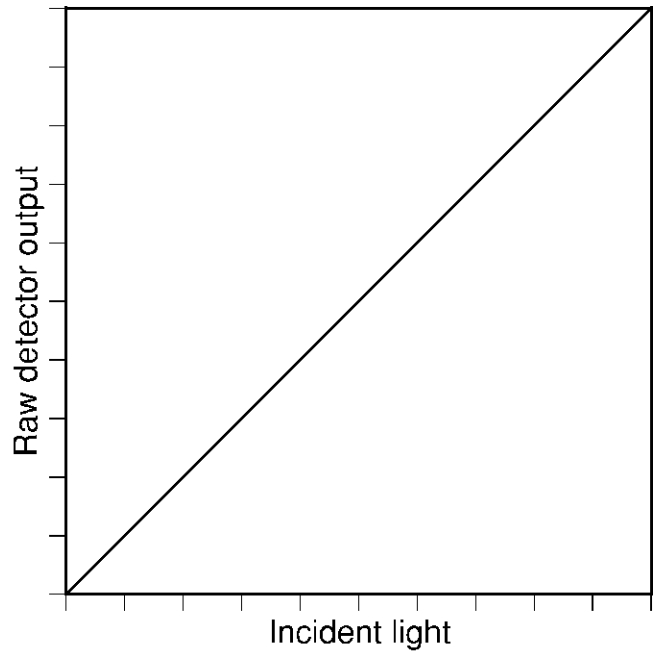


Figure 10. Relationship between incident light and raw detector signals for CCD arrays.

sual system than the other sensitivities shown in Figs. 6 and 7. The red sensitivity has its peak response coincident with the eye's L sensitivity.

Finally, it is worthwhile showing the spectral sensitivity of a typical color transparency film, shown in Fig. 9. Because of the inherent design of film in which sensitivities are stacked, limited choices for photosensitive materials, and a system that must simultaneously consider image capture and display, the spectral sensitivities do not closely resemble the human visual system. Furthermore, color-photographic materials are designed to make pleasing reproductions, not necessarily accurate reproductions. For all of these reasons, photographic reproductions are not color accurate although with experience, it is possible through filtration using color-compensating filters to achieve global color matches. This is done routinely in museum photographic departments.

CCD detectors have a linear response to incident light, shown in Fig. 10. This is a dramatic difference to the nonlinearity shown in Fig. 5. Depending on how the "raw" detector signal is processed and the digital properties of the stored image, this difference can be inconsequential or result in large visual artifacts. This will be considered in detail later in this article.

The raw detector signals, in the form of an analog signal, i.e., millivolts, are amplified and digitized using an analog-to-digital converter (ADC). The range of digital values depends on the number of bits in the ADC. Most commonly, 8, 12, or 16 bit ADC's are used. This means that there are 2^8 (256), 2^{12} (4096) or 2^{16} (65,536) number of gray levels for each color channel (also called "color levels" as well as "bit depth"). The greater the number of levels, the less the amount of error caused by the conversion from analog to digital signals. Visual artifacts caused by an insufficient number of gray levels are described and shown below in the next section.

Thus the camera has an inherent spatial and color resolution. The spatial resolution is determined in large

part by the number of detectors. For example, high-resolution scanning systems commonly have one-dimensional arrays with 6000 or 8000 detector elements that scan in 8000 or more steps. Thus the camera would have spatial resolution of 6000×8000 or 8000×8000 pixels ("picture elements"). This does not mean that a digital camera with more pixels is always better than one with less. Having many pixels combined with poor optics may have poorer image quality than fewer pixels with excellent optics. Ultimately, spatial resolution is determined for the entire camera system including the optics, sensor, and image processing, e.g., spatial interpolation, by imaging targets designed to quantify resolution and mathematically analyzing the digital images of these targets.^{2,13,19} Color resolution is determined by the number of bits in the ADC. For high-quality digital cameras, the ADC's have a minimum of 12 bits.

The Digital Image

A digital image is simply a two-dimensional array of numbers in which each number relates loosely to the amount of light reflected by an object. The image resolution defines the dimensions of the array. The concept of relating numbers to light reflection is easier to understand when a black and white, i.e., "monochrome" or "grayscale", image is considered. Essentially, dark areas have small numbers while light areas have large numbers. The most common bit depth for images is 8 bits per channel. Because digital values begin at 0, the numbers range from 0 to 255 ($2^8 - 1$). A white is near 255 while a black is near 0.

There is a tendency to treat digital values as if they were perceptions: a perfect white is 255, a perfect black is 0, and a medium gray, e.g., Kodak Gray Card, is 128. For color, all three channels have the identical digital values. Although it is always true that a larger number corresponds to a lighter gray, the relationship between digital values and perception is rarely one to one. Re-

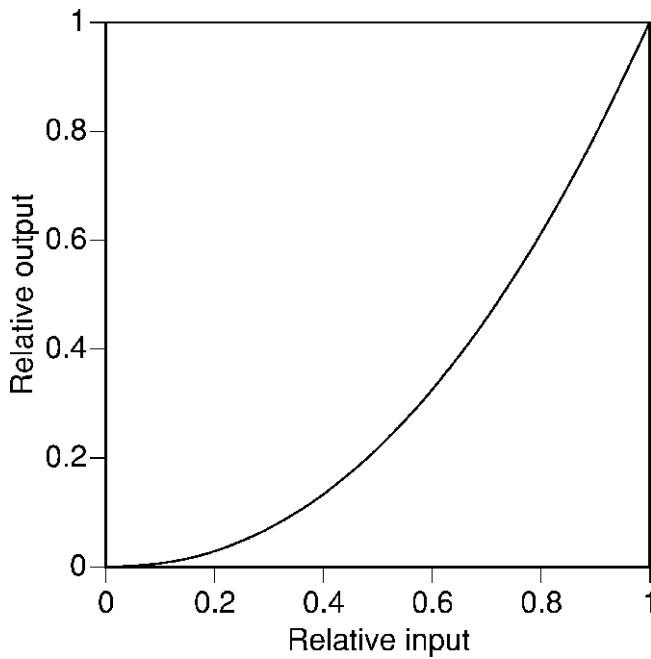


Figure 11. CRT nonlinearity. This nonlinearity is inherent to all vacuum tubes.^{20,21}

lating digital values to perception requires system characterization using standard test targets.

This difficulty in relating numbers to perceptions becomes further exacerbated when an image is output and viewed. Simply taking a digital image and displaying it on different computer platforms and printing it out on different printers reveals the large range of renditions that result from the identical image file. Again, this problem is minimized through system characterization using standard test targets and measurement equipment. The origins of this problem begin with the inherent nonlinearity of many imaging devices. Conventional photography, broadcast television, computer-controlled CRT and LCD displays, and printing all have a nonlinear relationship between their input, e.g., exposure, voltage, digital counts, dot area, and their output, measured as reflectance, transmittance, or light energy.

A specific nonlinearity worth exploring is the nonlinearity of CRT displays, shown in Fig. 11. By coincidence, this nonlinearity is similar to the human visual system, except inverted. This is an expansive function that is inherent to all vacuum tubes. During the early 20th century, a simple mathematical equation was derived to relate input and output, shown as Eq. 1.^{20,21} The normalized output was predicted by exponentiating the normalized input. The specific exponent is notated by the Greek symbol gamma, γ . The use of γ to notate an exponent stems from photographic science.²² However, a film's gamma has a different physical meaning than a display's gamma. Digital systems use gamma as shown in Eq. 1. This is a simplification. For very small digital counts, the exponent is replaced with a slope term, for example, sRGB.²³ Furthermore, this equation will only accurately model computer-controlled CRT displays if the monitor has its black level set perfectly: at 0 digital code value, there is not any emitted light while at 1 digital code value, light is emitted. Because this display set up is rarely achieved, more complex equations have been derived.^{24,25}

$$\left(\frac{\text{output}}{\text{maximum output}} \right) = \left(\frac{\text{input}}{\text{maximum input}} \right)^\gamma \quad (1)$$

Because CRT displays have inherent nonlinearity, raw detector signals from digital cameras will lead to poor image quality unless the image is first “gamma corrected,” that is, the inherent nonlinearity is appropriately compensated. The raw signals are exponentiated by the inverse of the display's gamma, shown in Eq. 2.

$$\text{output} = (\text{maximum output}) \left(\frac{\text{raw input}}{\text{maximum raw input}} \right)^{1/\gamma} \quad (2)$$

The net effect of gamma correcting the raw image and the display's inherent nonlinearity is an image that appears correct. That is, the tonal properties appear reasonable. Complete gamma correction is also a simplification. Quite often, gamma correction is not fully applied in order to compensate for dim (e.g., broadcast television) or dark, e.g., projected slides, viewing conditions reducing the perceived contrast in images. See Hunt²⁶ for greater details. This is shown in Fig. 12. Imposing an exponential function to a digital image is a common and useful procedure.

The vast majority of color images are 24-bit images, 8 bits for each of the red, green, and blue channels. Yet, for high-quality digital cameras, their analog-to-digital converters are 12 or 16 bits per channel. In order to have an 8-bit per channel image, the 4096 or 65,536 potential levels from the camera must be transformed to 256 levels. This is a reduction of information, and in similar fashion to spatial compression, this should be done in a manner that minimizes visual artifacts. The most common artifacts are banding in which smooth gradations become banded, or blocking in which details are lost, shown in Fig. 13. These are known as “quantization errors.” When a continuous signal, i.e., analog signal, becomes discrete, i.e., digital, it is quantized into a number of specific levels. The specific number of levels is determined by the bit depth. For all imaging applications, 2¹⁶ number of levels is a sufficient number of levels such that quantization errors are essentially eliminated. However, when converting to 8 bits per channel, quantization errors can be quite noticeable depending on the method of bit reduction. A numerical analysis is considered in a later section, **Optimal Encoding—Lightness**.

A useful method to analyze quantization is by evaluating image histograms. The histograms for the Fig. 13 images are shown in Fig. 14. The height of a peak represents the number of pixels with a particular digital value. The left-hand image has a histogram in which each level between the minimum and maximum digital counts has a number of pixels. Conversely, the right-hand image is missing data, resulting in only a few levels. The visual banding is quantified via an image histogram.

Assessing Color Image Quality

Obviously, any digital-capture system is capable of transforming an object into a digital image. The important question is whether the digital image has archival value as a digital representation. Can the digital values be used to estimate the color of the object? Even though any “picture tells a thousand words,” digital image-archives should do more; they should facilitate

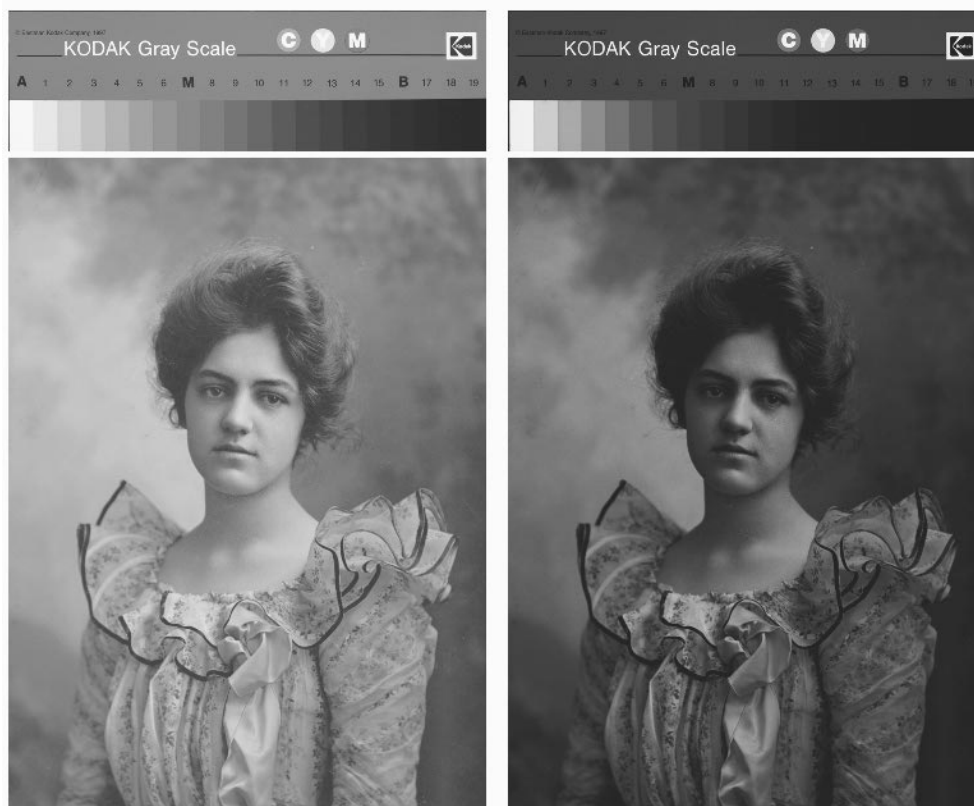


Figure 12. Photograph and gray scale imaged linearly and displayed with (left) and without (right) “gamma correction.” (Image courtesy of C. McCabe).



Figure 13. The effects of quantization on image quality is shown in the right-hand figure. Notice that smooth gradations become banded and that fine detail in the woman’s hair are lost.

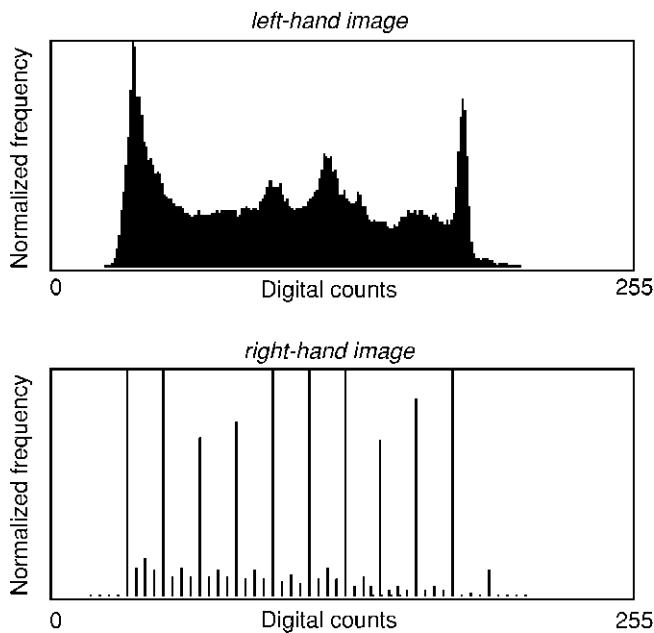


Figure 14. Histograms of the images shown in Fig. 13.

scientific documentation and study of works of art. The goal is to have the capability to estimate quantitative information about the object, not create a visually equivalent representation for a defined output device such as a display or printed document. Imaging test targets along with the work of art and comparing standard values of the test target with its estimates is most easily accomplished for analyzing the ability to estimate the color of cultural heritage. The standard values of interest are those that predict what observers see. CIELAB provides these required values.

Two types of test targets should be used. The first is a gray scale, such as the Kodak Gray Scale Q-13 or ISO 14524 chart.²⁷ Gray-scale targets characterize the relationship between digital values and lightness (by plotting the target's average digital counts and measured values), dynamic range (by evaluating whether each step has a unique average digital count), and whether the image is gray-balanced (by evaluating whether each channel has matched digital counts). Although it is common practice to include the Kodak Separation Guide along with a gray scale, this target cannot be used to effectively evaluate color errors or for color management. It was designed to validate the correct correspondence between four-color film separations and screens. This practice is unnecessary in modern graphic reproduction. Ideally, gray scale and color targets should span the lightness and color range of imaged objects and have similar spectral, i.e., made using similar colorants, and surface, i.e., gloss and texture, properties. For modern photographic and printed materials, IT8 standard targets are available.^{28,29} For paintings, targets are largely nonexistent. A target that is often used in broadcast television in order to evaluate the color accuracy of broadcast television cameras is the GretagMacbeth ColorChecker Color Rendition Chart (usually called the ColorChecker chart),³⁰ shown in Web Fig. 1 and Ref. 6. It is produced using painted papers. Because it has a number of pigments, it is a convenient target to evaluate the accuracy of digitized paintings. Both targets can be cut up to make smaller targets so that resolution is

not significantly reduced when including these targets along with the object undergoing digitization. The GretagMacbeth ColorChecker Color Rendition Chart is also available as a smaller target. A more comprehensive target of greater than 100 colored patches has also been recently released, the ColorChecker DC.

Both targets are first measured using a spectrophotometer, usually having bidirectional geometry, a geometry that minimizes specular reflection from contributing to the measured values.¹ From the spectral measurements, CIELAB values are calculated for a standard illuminant and observer, the specific standards dependent on the intent of the archive. The choice of illuminant and observer is complex. Should the object's color be defined by its appearance in an exhibition gallery, its appearance during conservation, or its appearance as envisioned by the artist? Exhibition galleries can have a range of illumination from bluish natural daylight (7500 K) to yellowish incandescent (2200 K). 7500 K and 2200 K refers to correlated color temperature, the temperature of a blackbody radiator which generates a white light matching the color of the source of interest. Sources and displays are often defined in terms of their correlated color temperatures. Conservators tend to use a combination of natural and artificial daylight, probably averaging to 6500 K. Depending on the artist, there can be one or more illumination choices, for example a *plein air* versus studio painter. Quite often, the image archive is defined by how the archive will be used rather than the above considerations. If the end product is a printed publication, CIE illuminant D50 and the 1931 standard observer are used.³¹ If the end product is web based, CIE illuminant D65 and the 1931 standard observer are used.²³ These output-oriented images should be considered derivative images, created using principles of color management.^{6,15,32} For the analyses in this article, CIE illuminant D65 and the 1964 standard observer were used because this corresponds to viewing objects in a natural-daylight lit studio with north-facing windows or typical conservation laboratories. In the author's experience, this combination leads to the best correlation between numerical and visual color quality because CIELAB is most visually uniform for D65 and metrics such as CIE94 are optimized for visual data subtending a 10° field of view, represented by the 1964 standard observer. Also, for metameric matching, the 1964 standard observer better correlates with visual observations. This combination of illuminant and observer is in contradiction with a number of imaging standards (e.g., Refs. 23, 31, and 32) that require the use of the 1931 standard observer and often illuminant D50.

Assuming that the digital-camera system is gray-balanced, the gray scale is used to ascertain whether the image is linear or nonlinear with respect to light input. Because CIELAB L^* is nonlinearly related to incident light as shown in Fig. 5, luminance factor, instead is used. Luminance factor, also known as CIE tristimulus value Y , is linearly related to incident light and is a standard of light measurement.¹¹ It is also used in the calculation of L^* . Spectrophotometers designed for color measurement provide both CIE tristimulus values, X , Y , and Z , and CIELAB coordinates. The average digital values for each patch from the two images of the Kodak gray scale shown in Fig. 12 are plotted against luminance factor in Fig. 15. As expected, the raw digital counts are linearly related to incident light. The gamma-corrected digital values are nonlinearly related to incident light. This nonlinearity can compensate for typical display

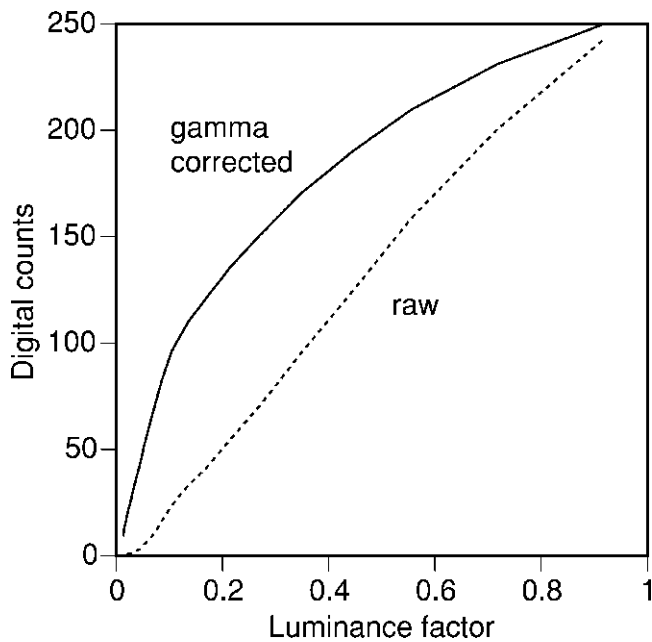


Figure 15. Luminance factor plotted against digital counts for the Kodak gray scales from Fig. 12.

nonlinearities, such as that shown in Fig. 11. This results in images that have reasonable tone reproduction, as demonstrated in Fig. 12. Because of various types of imaging noise, the curves are not perfectly smooth.

A scanback-type digital camera with spectral sensitivities similar to those shown in Fig. 6 was used to digitize the Kodak Gray Scale and ColorChecker chart. The raw signals were transformed to L^* , a^* , and b^* coordinates, the general methodology described below, **Optimal Encoding – Color**. Both numerical and graphical analyses are performed in order to evaluate the camera’s accuracy in estimating colorimetric data measured using a spectrophotometer. Graphically, “vector plots” are made, shown in Fig. 16. The uppermost portion of Fig. 16 is an a^*b^* projection. The end of the tail represents the measured coordinates while the head represents the estimated coordinates. Vectors pointing either towards or away from the origin (the center of the dashed lines at $a^* = 0$, $b^* = 0$) indicate chroma error. Chroma is defined as the degree of departure of a color from a gray of the same lightness.⁶ Vectors pointing away from the origin indicate the estimate is over-predicting chroma. Vectors pointing towards the origin indicate the estimate is under-predicting chroma. Vectors pointing in directions other than towards or away from the origin indicate hue errors. The length of the vector indicates the magnitude of the chromatic error. Ideally, the errors should be sufficiently small such that only the arrowhead is shown without a tail. There are some systematic trends: yellows have large chroma errors, blues have large hue errors, and reds and greens have relatively smaller errors. The bottom graph of Fig. 16 shows an $L^*C^*_{ab}$ projection where C^*_{ab} represents chroma ($\sqrt{a^{*2} + b^{*2}}$). Vectors that are pointing upwards indicate that the estimation is too light; vectors pointing downward indicate that the estimation is too dark. Vectors parallel with the C^*_{ab} axis indicate accurate lightness estimation. There are two systematic trends. First, many of the chromatic samples’ lightnesses have been underestimated because the vectors are point-

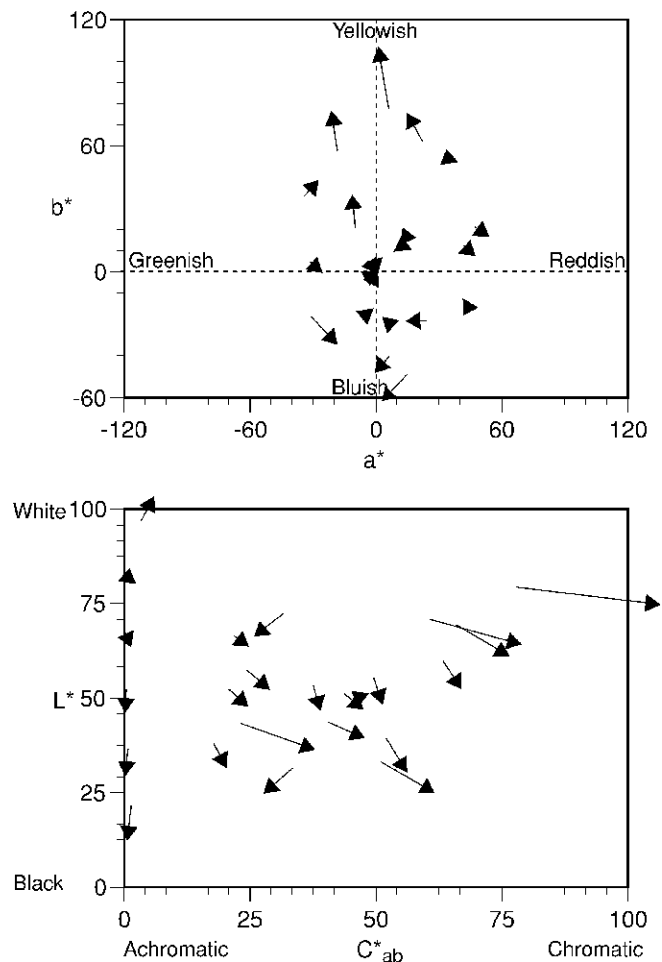


Figure 16. CIELAB vector plots in which the arrowhead defines the coordinates of the estimated values while the end of the arrow tail defines the coordinates of the measured values.

ing downwards. Second, the lighter samples of the ColorChecker’s gray scale have been over estimated (vectors pointing upwards) and the darker neutrals have been under estimated (vectors pointing downwards). Ordinarily, errors of this type for neutral samples indicate calibration errors in which there is a mismatch between actual and assumed photometric properties of the image capture system, that is, a mismatch in gamma. In this case, these estimation errors were caused by spatial non-uniformities in illumination. Non-uniform illumination of the Kodak gray scale was interpreted as a slight non-linear photometric response. This was compensated for during color management. Because the spatial non-uniformities varied across the image plane, this compensation resulted in systematic errors in different image locations.

These differences are quantified numerically by calculating differences in color positions. CIELAB is a rectangular color space with L^* , a^* , and b^* axes (shown in Fig. 4). Thus ΔL^* , Δa^* , and Δb^* values are calculated where the Greek symbol Δ (“delta”) represents difference. ΔL^* is calculated by subtracting the measured value from the estimated value, i.e., $\Delta L^* = L^*_{\text{estimated}} - L^*_{\text{measured}}$, and in similar fashion for the other coordinates. A positive Δ value indicates that the estimated value has more of the particular quantity than the measured value. It is also useful to describe differences in

TABLE I. Colorimetric Errors Comparing Measured and Estimated Values for a GretagMacbeth ColorChecker Color Rendition Chart Imaged with a Scanback-Type Digital Camera Followed by Color Management

Sample	ΔL^*	Δa^*	Δb^*	ΔC^*_{ab}	ΔH^*_{ab}	ΔE^*_{ab}	ΔE^*_{94}
Dark Skin	-6.0	-0.3	3.6	2.5	-2.6	7.0	6.5
Light Skin	-2.6	4.1	-0.4	2.6	3.2	4.9	3.8
Blue Sky	-4.2	0.5	-3.9	3.7	-1.3	5.8	4.7
Foliage	-6.8	-1.4	14.9	14.5	4.0	16.5	10.3
Blue Flower	-4.9	-1.0	-4.7	4.3	2.1	6.8	5.5
Bluish Green	-5.8	5.2	-4.6	-5.6	-4.2	9.1	6.9
Orange	-7.0	-0.8	4.5	3.4	-3.1	8.4	7.2
Purplish Blue	-4.1	-6.6	-7.5	6.9	7.1	10.7	6.5
Moderate Red	-3.8	4.8	-4.3	3.7	5.3	7.5	5.1
Purple	-6.4	-8.8	-0.3	-5.4	7.0	10.9	8.2
Yellow Green	-6.5	-2.5	18.0	18.0	2.7	19.3	8.2
Orange Yellow	-8.2	-7.1	12.6	10.2	-10.2	16.7	10.0
Blue	-8.1	-11.7	-12.5	10.4	13.6	18.9	11.6
Green	-6.5	6.4	7.0	1.6	9.3	11.5	8.5
Red	-8.7	6.0	-4.2	4.0	6.1	11.3	9.4
Yellow	-4.6	-4.8	28.5	28.2	-6.1	29.3	8.3
Magenta	-3.3	-1.1	-1.8	-0.3	2.1	3.9	3.5
Cyan	-6.3	12.1	-12.7	1.3	-17.5	18.6	12.9
White	6.1	-3.9	1.1	2.4	-3.2	7.3	7.1
Neutral 8	1.5	0.6	-1.7	0.2	1.8	2.3	2.3
Neutral 6.5	-3.3	0.5	-1.2	1.1	0.7	3.5	3.5
Neutral 5	-5.7	0.3	-0.5	-0.2	-0.5	5.8	5.8
Neutral 3.5	-6.6	0.7	0.4	-0.5	-0.6	6.7	6.7
Black	-8.8	0.6	1.1	-0.8	-0.9	8.8	8.8
Average	-5.0	-0.4	1.3	4.4	0.6	10.5	7.1
Maximum						29.3	12.9

lightness, chroma (ΔC^*_{ab}), and hue (ΔH^*_{ab}), rather than lightness, redness/greenness, and yellowness/blueness, particularly for chromatic samples. The equations are given in Refs. 6 and 11. All of these values have been tabulated in Table I. With experience, the numerical information can be quite useful. In many cases, the graphical information is more intuitive.

An obvious question concerns the magnitude of error. Are these errors large or small? Are they visible? Are they objectionable? Simply stated, these errors are large and objectionable, particularly since the goal is to estimate colorimetry from an image archive. One problem is the systematic nature of some of the errors shown in Fig. 16. The second problem is the size of these errors. When all three dimensions are considered simultaneously, the length of the vector can be used as an error metric. In CIE terminology, this is called a total color difference and is notated by ΔE^*_{ab} . However, CIELAB as a color-difference space is poorly correlated with visual judgments of color difference.⁶ The last column in Table I lists a weighted color difference, ΔE^*_{94} , also referred to as CIE94. This equation was designed for industries manufacturing colored products.³³ The weighting was optimized to improve correlation with visual tolerances. A CIE94 color difference of unity is slightly above a visual threshold. Thus, if pairs of colored patches were prepared with these differences in their CIELAB coordinates, the differences would all be obvious, simulated in Web Fig. 2.

It is important to point out that CIE94 was designed to correlate with comparisons of the quality of colored patches, not colored images. As a rule of thumb, two pictorial images viewed side by side with systematic errors that result in an average ΔE^*_{ab} of 2.2 or less are indistinguishable from one another.^{34,35} If the errors are

around $5\Delta E^*_{ab}$ on average, the accuracy is acceptable for high-quality color reproduction. However, the 2.2 and $5\Delta E^*_{ab}$ rule of thumb applies to imaging **systems** where errors from both image input and output occur. Because this analysis is only considering image input, the errors should be even smaller. In the author's opinion, a well-designed image input device should result in average errors of less than $2\Delta E^*_{ab}$ for the ColorChecker. Presently, there has been insufficient evaluation of CIE94's effectiveness for predicting the color quality of pictorial images and accordingly, recommended figures of merit cannot be given. Also, this equation will soon be updated by the CIE.

As a final analysis, a color-difference histogram should be evaluated, shown in Fig. 17. Quite often, differences are not normally distributed and average and maximum errors can be misleading.

Despite color management, these errors are large although not unexpected. It is not surprising given the large discrepancy between the camera and human spectral sensitivities, plotted in Fig. 6. Although the camera does a fine job in recording red, green, and blue light, the human visual system does not "record" light in the same manner. No matter how complex the color management system, there will always be estimation errors.

Optimal Encoding – Lightness

From the review of digital imaging, minimizing quantization errors is critical in order to maximize an archive's scientific value. This is achieved by the optimal encoding of the lightness properties of the work of art. The first step towards optimization is by review of the proper digital capture practices for two-dimensional works of art and documents, listed in Table II.

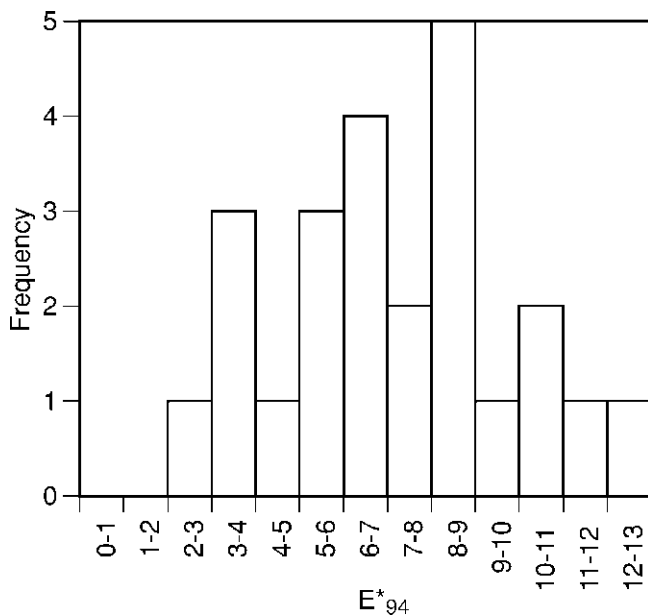


Figure 17. CIE94 histogram of the data given in Table I.



Figure 18. Incorrect exposure time or an insufficient amount of light results in excessive image noise, shown for the blue channel.

TABLE II. List of Proper Digital Capture Practices

Object and image planes parallel
Correct camera aperture for appropriate depth of field
Spatially uniform illumination across the object
Sufficient amount of illumination
Amount of ultraviolet and infrared radiation minimized (or eliminated by filtering)
Flare (stray light) minimized
Specular reflections minimized
Digital cropping minimized
Characterization targets included along with object
Exposure time appropriate to maximize dynamic range of raw digital data
Exposure times or amplification for each channel appropriate to yield gray balance

Many of these practices are consistent with proper conventional photographic practices. It is worth stressing the importance of having sufficient illumination and the maximum aperture to keep exposure (scan) times short. With an increase in exposure time, noise accumulates.¹³ This is observed most easily by evaluating the blue channel in dark image areas. Noise appears as a random speckled pattern, shown in Fig. 18. The blue channel is used because CCD detectors have their poorest sensitivity to the blue region of the visible spectrum, and therefore are most affected by noise accumulation, particularly when incandescent illumination is used. From a conservation perspective, minimizing exposure times is also desirable, often a problem with scanbacks.⁴ Techniques to evaluate image noise in digital capture are described in Refs. 2, 13, 36, and 37.

In conventional photography, many films are “very forgiving” if the image is either under- or over-exposed. Because most films are designed for photographing scenes with very large dynamic ranges, there is more exposure latitude when capturing paintings. CCD detectors have less exposure latitude; an incorrect exposure is “less forgiving.” If the exposure time is too long, the CCD array saturates causing blooming. A specular highlight smears in the direction of the one-dimensional array. Also, light areas are clipped, mapped to the same maximum value, resulting in a loss of highlight information. If the exposure time is too short, the raw data do not encompass the full range of possible digital values. This results in quantization error.

A technique to evaluate the effects of quantization on color quality is to define an imaging system, assume that there is 1 bit of uncertainty (accomplished by adding 1 bit to the signal), and evaluate the effect of this uncertainty on colorimetric error.³⁸ For this analysis, only ΔL^* errors were considered based on analyzing the Kodak gray scale. If the raw camera data were 16 bit and the digital image encompassed the full possible dynamic range (0 – 65,535), there would not be any significant error as shown in Table III. When the quantization is reduced to 12 bits, errors appear, largely for the darker samples. The 10-bit (0 – 1023) level of error could be observable in smoothly varying colors. At 8 bits (0 – 255), there are large errors, particularly for dark colors. If exposure times are too short, this is equivalent to reducing the bit depth. Thus the 10 and 8 bit data shown in Table III correspond to the effects of underexposure using a digital camera. Digital uncertainty from linear signals has a greater visual effect for dark colors. The systematic trend, in which errors increase with decreasing lightness, is explained by the human visual system’s nonlinear lightness response, shown in Fig. 5. An error of one bit for a dark color results in a larger visual difference in lightness than a one-bit error

TABLE III. The Effects of Quantization Levels on Lightness Errors, ΔL^*

Kodak gray scale	L^*	ΔL^* for 16 bits	ΔL^* for 12 bits	ΔL^* for 10 bits	ΔL^* for 8 bits
19	11.70	0.01	0.15	0.47	2.22
18	11.86	0.01	0.15	0.50	2.22
17	14.27	0.01	0.13	0.50	1.93
B	16.54	0.01	0.11	0.50	1.72
15	19.43	0.01	0.09	0.49	1.43
14	21.53	0.01	0.08	0.48	1.33
13	25.46	0.00	0.07	0.47	1.05
12	27.63	0.00	0.06	0.46	0.95
11	31.41	0.00	0.05	0.45	0.82
10	35.09	0.00	0.04	0.44	0.70
9	38.62	0.00	0.04	0.43	0.62
8	43.56	0.00	0.03	0.42	0.52
M	48.08	0.00	0.03	0.41	0.45
6	53.35	0.00	0.02	0.40	0.38
5	59.17	0.00	0.02	0.39	0.32
4	65.66	0.00	0.02	0.39	0.28
3	72.53	0.00	0.01	0.01	0.24
2	79.37	0.00	0.01	0.35	0.20
1	87.88	0.00	0.01	0.41	0.17
A	96.63	0.00	0.01	0.01	0.14
Average ΔL^*		0.00	0.06	0.40	0.88
Maximum ΔL^*		0.01	0.15	0.50	2.22

for a light color. This is seen in the 8 bit data. The errors decrease with increasing lightness of the gray scale. This would result in large banding, especially in shadows and dark colors. Shadow detail would also be lost. Clearly, it is critical to set the exposure time properly.

Based on this simple analysis, a camera's analog to digital converter should have a minimum of 12 bits. This is in agreement with Olson³⁹ who found that quantization errors should result in a maximum ΔL^* of 0.25 or less. His analysis accounted for both the human visual system's color and spatial properties. Hill⁴⁰ performed an extensive computational analysis for theoretical and actual color gamuts and also concluded that linear encoding required 11 or 12 bits.

As Table III shows, 8-bit quantization results in large visual errors for linear signals. However, when 12 or 16 bit data are transformed to 8 bit per channel data, there isn't a restriction that the transformation be linear. It was noted above that by coincidence, the nonlinearities of CRT displays are nearly the exact inverse of the human visual system's nonlinearity (seen by comparing Figs. 5 and 11). As a consequence, gamma correcting signals as part of the bit-reduction transformation has the "free" benefit of reducing visual errors. This is shown in Table IV in which 12 bit signals encompassing the full dynamic range (0 – 4095) are gamma corrected [i.e., Eq. 2] before being mapped to 8 bits. Mapping linear 12-bit raw signals nonlinearly onto 8-bit signals is clearly advantageous. The level of improvement is equivalent to increasing bit depth.

The relationship between incident light, gamma-corrected signals, and normalized lightness, i.e., CIE $L^*/100$, are plotted in Fig. 19. All these curves have similar shape; their differences are not significant in terms of how the encoding affects quantization errors. As a comparison, a Kodak gray scale was photographed using 4" x 5" positive film in a museum photographic department, then digitized using a drum scanner with a linear response. The relationship between incident light

TABLE IV. The Effects of Gamma on Lightness Errors, ΔL^* . (See text for an explanation of the computations.)

Kodak gray scale	L^*	ΔL^* for $\gamma=3$	ΔL^* for $\gamma=2.5$	ΔL^* for $\gamma=2$	ΔL^* for $\gamma=1$	ΔL^* for scanned photography
19	11.70	0.00	0.00	0.01	2.22	1.43
18	11.86	0.03	0.04	0.08	2.22	1.43
17	14.27	0.17	0.20	0.27	1.93	1.31
B	16.54	0.23	0.26	0.34	1.72	1.13
15	19.43	0.29	0.31	0.38	1.43	1.01
14	21.53	0.31	0.33	0.39	1.33	0.92
13	25.46	0.35	0.36	0.40	1.05	0.76
12	27.63	0.36	0.37	0.41	0.95	0.69
11	31.41	0.38	0.38	0.40	0.82	0.59
10	35.09	0.39	0.39	0.40	0.70	0.49
9	38.62	0.40	0.39	0.39	0.62	0.43
8	43.56	0.41	0.39	0.38	0.52	0.34
M	48.08	0.42	0.39	0.37	0.45	0.27
6	53.35	0.42	0.39	0.36	0.38	0.21
5	59.17	0.43	0.38	0.35	0.32	0.17
4	65.66	0.43	0.38	0.34	0.28	0.18
3	72.53	0.43	0.38	0.32	0.24	0.24
2	79.37	0.43	0.37	0.31	0.20	0.32
1	87.88	0.43	0.37	0.30	0.17	0.40
A	96.63	0.44	0.36	0.29	0.14	0.46
Average ΔL^*		0.34	0.32	0.32	0.88	0.64
Maximum ΔL^*		0.44	0.39	0.41	2.22	1.43

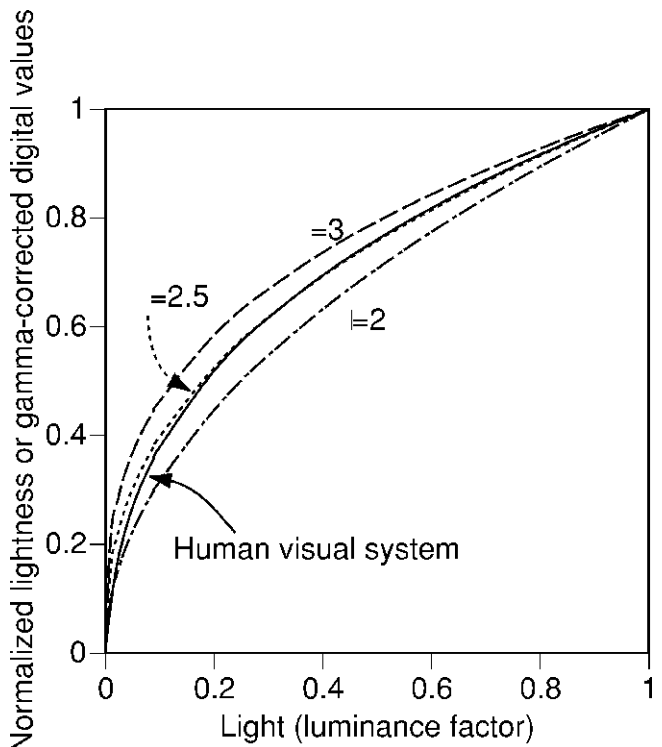


Figure 19. Relationship between light, expressed as luminance factor, and lightness (solid line) or gamma-corrected signals ($\gamma=3$: dashed line; $\gamma=2.5$: dotted line; $\gamma=2$: dot-dashed line).

and raw 12-bit signals is plotted in Fig. 20. This nonlinearity is typical of conventional photography, though quite different than what is usually shown as the nonlinear response of film. This is for two reasons: linear signals are plotted rather than logarithmic signals and when photographing paintings using controlled

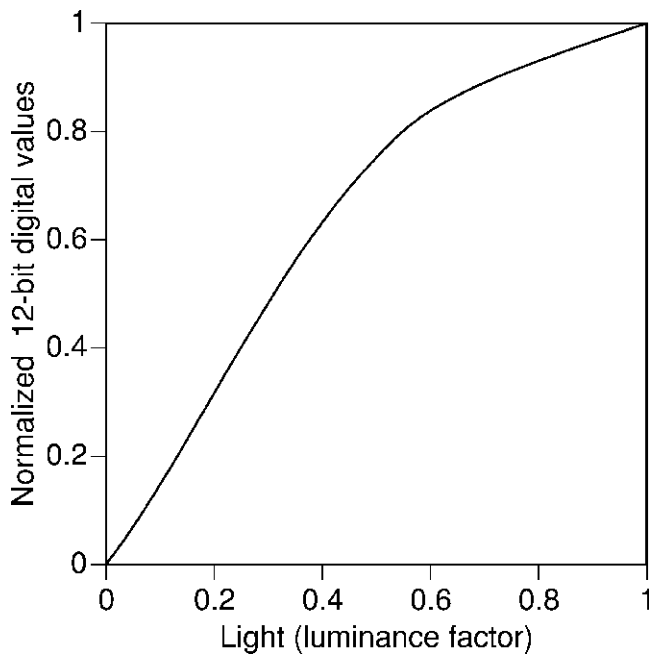


Figure 20. Relationship between light, expressed as luminance factor, and normalized 12-bit raw signals for a digitized photographic positive transparency.

illumination, the full dynamic range of conventional film is not utilized. These data were used to perform a quantization error analysis in which the photographic nonlinearity was used rather than a gamma function in transforming 12-bit to 8-bit per channel data, also shown in Table IV. The photographic nonlinearity has much larger error than any of the gamma-corrected signals. That is, the digitized photographic transparency resulted in greater quantization errors than direct digital capture.

There are several different gamma functions used in the imaging industry. These can be either *de facto* or legitimate national or international standards. Choices include 1.8, the system gamma of Apple computer systems; 2.2, the inherent nonlinearity of CRT displays when modeled by Eq. 1 and recently incorporated into the sRGB display encoding;²³ 3.0, the nonlinearity incorporated into CIELAB;¹¹ 2.3, an empirical fit to CIE L^* used in the RLAB color-appearance model.⁴¹ The CIE L^* equation, $L^* = 116(Y/Y_n)^{1/3} - 16$ where Y is luminance factor of a stimulus and Y_n is the luminance factor of the white object-color stimulus, has an offset term. If the offset is removed and the following equation is fit: $L^*/100 = (Y/Y_n)^{1/\gamma}$, a gamma of 2.3 results when the independent data are uniformly sampled by L^* (i.e., $Y/Y_n = 0.00, 0.01, 0.03, 0.06, 0.11 \dots$) and 2.4 when the independent data are uniformly sampled by Y/Y_n (i.e., $Y/Y_n = 0.00, 0.10, 0.20, 0.30, 0.40 \dots$). When an offset is included, the sRGB exponent is 2.4. The analyses shown in Tables III and IV were repeated. For $\gamma = 1.8$ the average error was $0.35 \Delta L^*$; for the other exponents, the average was 0.34. These differences were not statistically significant, therefore, the particular exponent is not critical.

The above analyses lead to the following recommendations. First, the digital range of the raw data should be maximized, but without clipping. For 12-bit data, the maximum digital values should not exceed about 4000, likely specular highlights. For sample A of the Kodak

Gray Scale, the average digital value should be around 3900. For 16-bit data, the maximum digital values should not exceed about 64,000 and sample A of the Kodak Gray Scale should have an average digital value of about 63,000. When writing images in standardized formats such as TIFF, the raw data should be directly saved as 16-bit TIFF. For 12-bit data, the digital values are premultiplied by 2^4 , i.e., they are bit shifted so that the images can be viewed in Photoshop™ without adjustment. This does not affect quantization errors. If this premultiplication (bit shifting) is not performed the displayed image will be very dark. For 8-bit TIFF, the raw data must be rescaled and gamma corrected. The maximum digital value should not exceed about 250. The National Archives and Records Administration specifies digital values of 247 and 8 for patches A and 19, respectively of the Kodak Gray Scale.⁴² For sample A of the Kodak Gray Scale, the average digital value should be around 245. The minimum values for all bit depths should approach 0. However, for a variety of computational and image noise reasons, the values for sample 19 of the Kodak Gray scale will be about 5, 80, or 1000 for 8-, 12-, and 16-bit data, respectively. The key is ensuring that the available range of digital values is maximized during image acquisition but without clipping. That is, it is critical to achieve proper exposure. If software is available to display raw data histograms, this can provide the needed information. Proper exposure should not be verified by looking at the digitized image on a monitor. Because the display is 8 bits per channel, camera software will have user controlled adjustments to impose a transfer function, sometimes called a “process curve”, to convert from raw to display data. The same curve will be used to generate the 8 bit TIFF file. Although the image may look reasonable, quantization error is still being introduced.

Optimal Encoding – Color

Dealing with color is significantly more complex than optimally encoding lightness. As described above, most digital cameras in use today have inappropriate spectral sensitivities. If the sensor was optimized for photographic materials, shown in Fig. 6, or for consumer applications, shown in Fig. 7, they are not accurate color measurement instruments. For scientific imaging, the camera should be thought of as an imaging colorimeter or spectrometer. Several systems have been designed as imaging colorimeters: the IBM Pro 3000 system,^{43–45} the VASARI system,^{46,47} and the MARC system.⁴⁸ Systems designed as imaging spectrometers are still at the research and development stage, summarized in Refs. 49, 50 and 51.

An experiment was performed to evaluate the colorimetric potential of four imaging systems, three digital cameras and scanned conventional photography. Camera A has spectral sensitivities closely related to the human visual system, similar to those shown in Fig. 8. It consists of a monochrome sensor and three color filters. Camera B has spectral sensitivities similar to those shown in Fig. 7. It consists of a two-dimensional color CCD array. Camera C has spectral sensitivities similar to those shown in Fig. 6. It is a scanback employing a flat-bed scanner-type trilinear color-filter array. An 8” × 10” view camera along with tungsten-balanced chrome 64 ISO film was used for conventional photography. Color compensation filters were used to achieve a visual color match between neutral areas of the test target and its reproduction. The transparency was digitized

using a flat-bed scanner with densitometric spectral sensitivities similar to Fig. 6. The illumination for all four systems was tungsten halogen with a correlated color temperature around 3200 K. Image capture was performed adhering to the practices outlined in Table II. All four digital systems have 12-bit analog to digital converters. The raw signals were recorded as 16-bit TIFF uncompressed. There was not any signal processing such as gamma correction imposed. Thus, these images were “linear RGB.” However, because of differences in spectral sensitivity, light sensitivity (dynamic range), the spectral characteristics of tungsten illumination, and flare, the range of digital values were quite different for each channel and for each imaging system.

Three targets were imaged: the Kodak Gray Scale, the GretagMacheth ColorChecker Color Rendition Chart, and a custom target of 68 artist oil paints, shown in Web Fig. 3. Each of the paints was mixed with titanium white in order to maximize the spectral “fingerprint” of a given pigment. The Kodak Gray Scale and ColorChecker chart were used to derive a transformation from R, G, and B to L^* , a^* , and b^* values. The paint target was used to evaluate the accuracy of the transformation. The transformation can be thought of as employing color management principles.

The first step was to develop a transform that linearized the raw data with respect to CIELAB. The general equation is shown as follows:

$$L^* = k_{g,2} \left(k_{g,1} \frac{d}{65,535} + (1 - k_{g,1}) \right)^\gamma + k_o \quad (3)$$

where L^* is the measured L^* values of the Kodak Gray Scale, d is either the average raw R, G, or B digital values of each gray scale sample, and the remaining terms are model coefficients. This particular equation enables amplification ($k_{g,1}$), properties of the ADC ($d/65,535$), flare (k_o), and differences in measurement geometry between the spectrophotometer used to measure the gray scale and the digital capture system ($k_{g,2}$) to be taken into account. In most cases, not all of the model terms were statistically significant and the equation was reduced in complexity accordingly. This equation can be thought of as a more analytical form of the exponential model described by Eq. 1. Nonlinear optimization was used to estimate the model parameters for each channel and for each camera. The camera signals, linearized with respect to L^* , are referred to as R^* , G^* , and B^* . Equation 3 also facilitates gray balance. In the case of digitized conventional photography, a different approach was taken to linearize the raw signals because the nonlinearity shown in Fig. 22 cannot be well fit using Eq. 3. A fifth-order polynomial was used, Eq. 4:

$$L^* = 100 \left(\beta_0 + \beta_1 \left(\frac{d}{65,535} \right) + \beta_2 \left(\frac{d}{65,535} \right)^2 + \beta_3 \left(\frac{d}{65,535} \right)^3 + \beta_4 \left(\frac{d}{65,535} \right)^4 + \beta_5 \left(\frac{d}{65,535} \right)^5 \right) \quad (4)$$

where $\beta_0 - \beta_5$ are model coefficients estimated by linear optimization.

The average R^* , G^* , and B^* values of each color patch of the ColorChecker were used to develop a linear transformation, Eq. 5:

$$\begin{aligned} \hat{L}^* &= \beta_{1,1}R^* + \beta_{1,2}G^* + \beta_{1,3}B^* \\ \hat{a}^* &= \beta_{2,1}R^* + \beta_{2,2}G^* + \beta_{2,3}B^* \\ \hat{b}^* &= \beta_{3,1}R^* + \beta_{3,2}G^* + \beta_{3,3}B^* \end{aligned} \quad (5)$$

where each β term is a model coefficient. Hats (“^”) are shown over the CIELAB values because these are estimated values. The model coefficients were constrained via Eq. 6:

$$\begin{aligned} \beta_{1,1} + \beta_{1,2} + \beta_{1,3} &= 100 \\ \beta_{2,1} + \beta_{2,2} + \beta_{2,3} &= 0 \\ \beta_{3,1} + \beta_{3,2} + \beta_{3,3} &= 0 \end{aligned} \quad (6)$$

The purpose of Eq. 6 was to maintain gray balance. The model parameters for each camera were estimated using least-squares linear optimization. A numerical example of this approach to color management is presented in Ref. 6. This is referred to as a colorimetric transformation. Although polynomial expansions of Eq. 5 are often used for color management, these often do not result in improved performance when independent data are evaluated.

Before evaluating the independent data, the oil paint target, it is useful to evaluate the modeling performance of the Kodak Gray Scale and ColorChecker chart. The average CIE94 color difference between measured and estimated values for the Gray Scale varied between 0.5 and 1.0. The estimation performance for the ColorChecker chart is shown in Figs. 21 and 22. As expected, the closer the camera’s spectral sensitivities are to the human visual system, the better the colorimetric estimation. The causes for the large errors for camera C were discussed above. The errors for cameras A and B are random indicating that this simple transformation is performing appropriately. It was surprising that the performance for camera B was not better. The MARC system, having similar spectral sensitivities, has a reported⁴⁸ estimation error of $2.5\Delta E^*_{ab}$ for the ColorChecker whereas for this analysis, the average was $6\Delta E^*_{ab}$. Further analyses revealed that the colorimetric performance was very sensitive to the illumination system’s spectral power distribution, spatial uniformity, and illuminance, as well as setting the optimal exposure time. Prefiltering the source in order to balance the three channels and improve its daylight characteristics, numerical flat-fielding in order to improve spatial uniformity, signal averaging, and more careful attention to exposure reduced the average estimation error to $3.5\Delta E^*_{ab}$. The Marc I camera employed a Sony ICX021AK sensor whereas camera B employed a Sony ICX085AK sensor. The latter sensor has improved light sensitivity but its spectral sensitivities are poorer approximations to the human visual system. Thus, the reduction in estimation accuracy from 2.5 to $3.5\Delta E^*_{ab}$ is consistent with these differences. All of the camera systems’ colorimetric estimation accuracies were highly dependent on image capture characteristics underscoring the importance of proper capture procedures listed in Table II. The colorimetric accuracy of digitized film was intermediate between cameras B and C, consistent with film’s spectral sensitivities shown in Fig. 9.

The estimation accuracy for the artist oil paint target is shown in Figs. 23 through 25. The trends for the direct

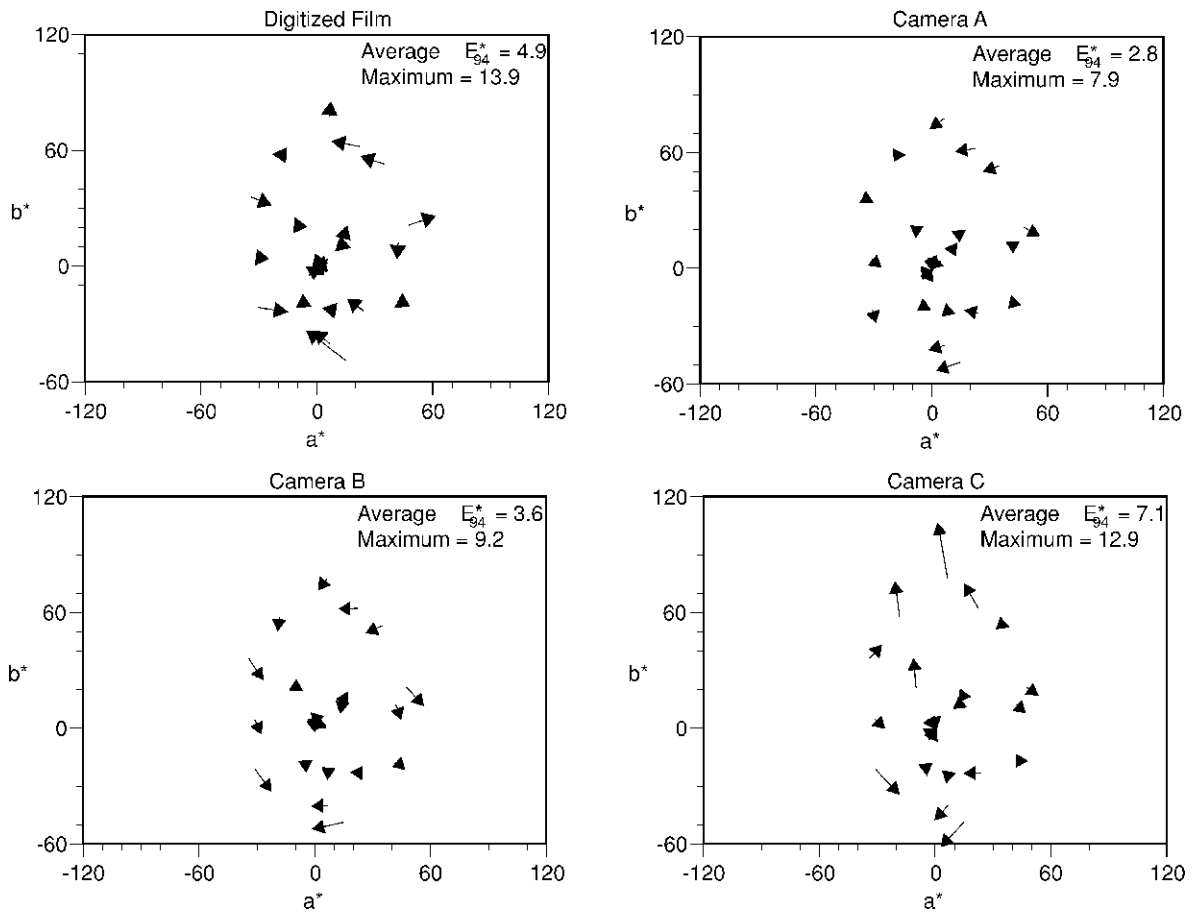


Figure 21. CIELAB a^*b^* projection vector plots showing estimation errors for the ColorChecker chart.

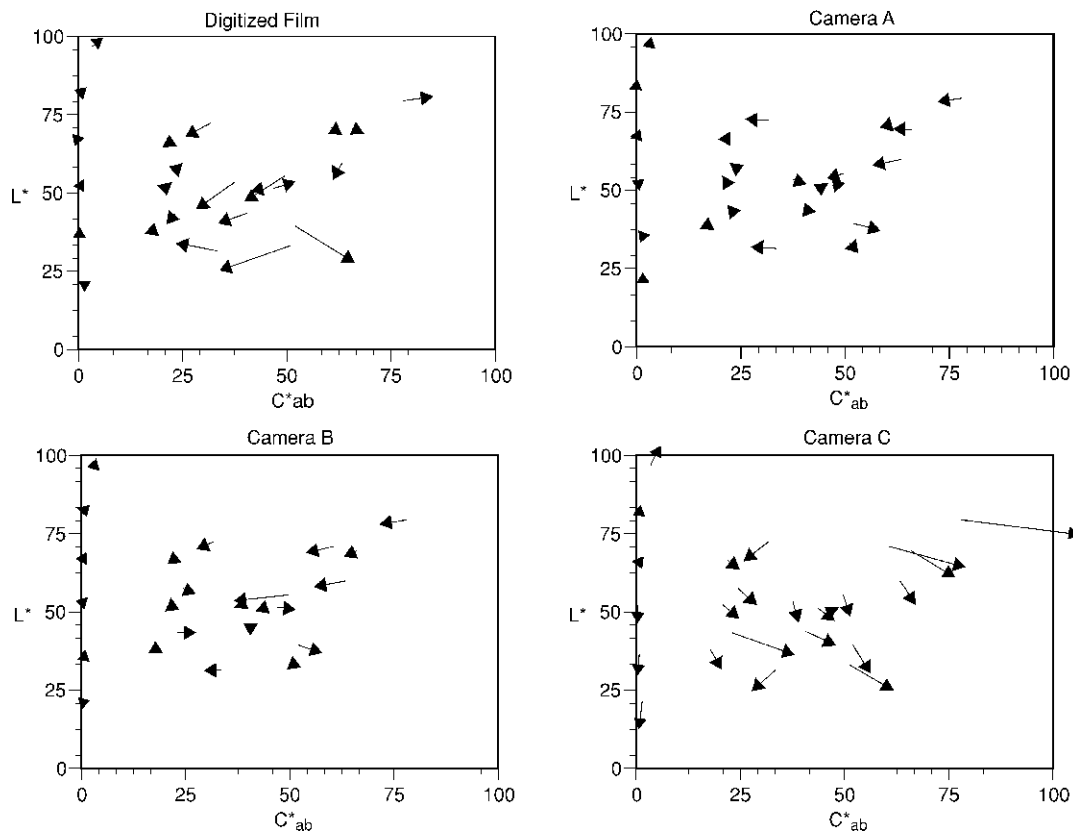


Figure 22. CIELAB $L^*C^*_{ab}$ projection vector plots showing estimation errors for the ColorChecker chart.

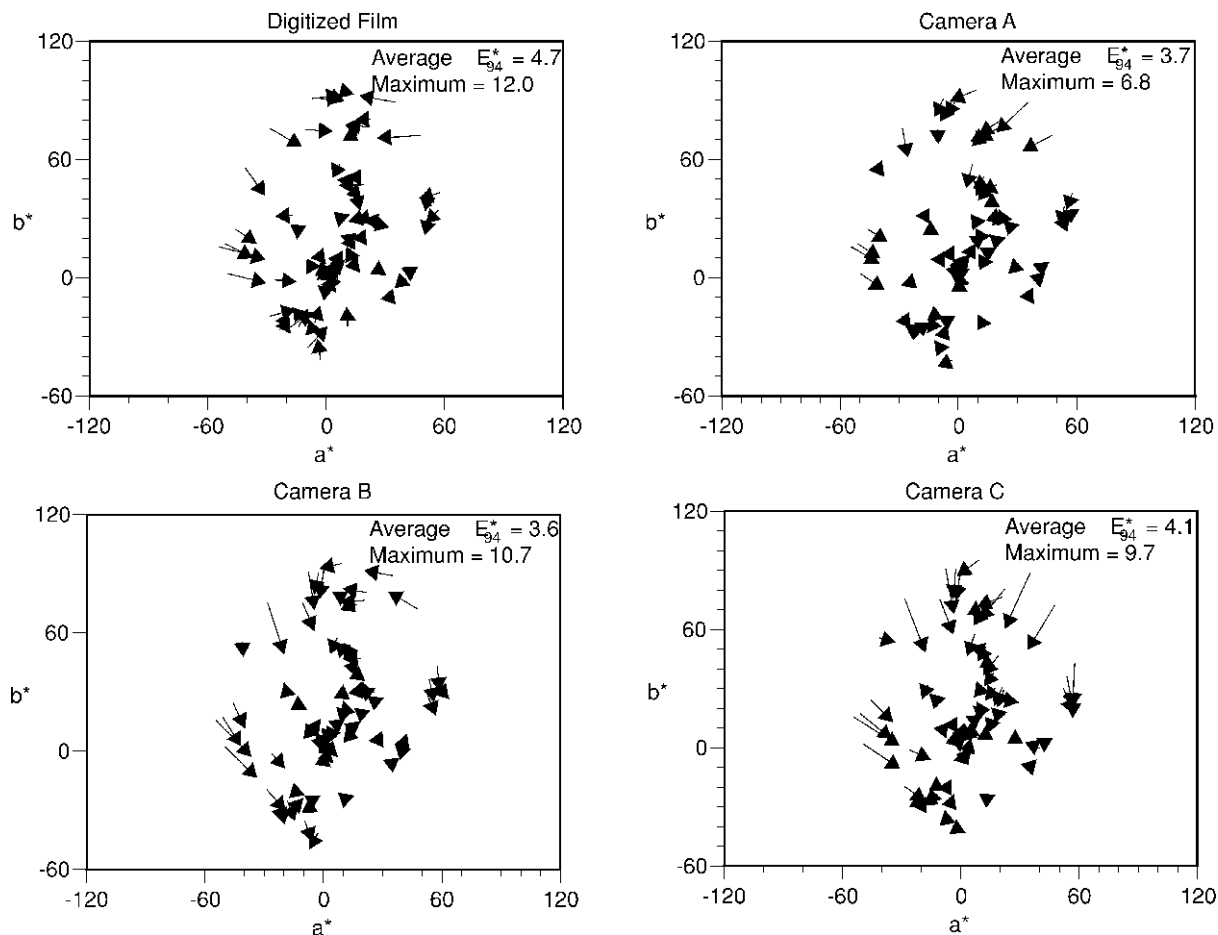


Figure 23. CIELAB a^*b^* projection vector plots showing estimation errors for the artist oil target.

digital capture systems were the same as the ColorChecker accuracy: Camera A had the least estimation error while camera C had the greatest estimation error. The digitized photographic system had the poorest estimation accuracy of the four imaging systems. For each imaging system, there were systematic errors; that is, certain color regions were not accurately estimated. This is observed by evaluating the error vectors. For example, the $+a^*+b^*$ and $-a^*-b^*$ quadrants had vectors pointed in similar directions for camera C. Lightness was underestimated for the scanned photographic system. Ideally, error vectors should be largely random and small, such as those shown for the ColorChecker in Fig. 21. Because CIELAB is not visually uniform, caution should be taken when evaluating error-vector plots. The same length vector corresponds to a different visual difference depending on the chroma of the measured color. Thus, the overall accuracy is judged by looking at the histograms plotted in Fig. 25. Clearly, camera A has the highest estimation accuracy. One important property is to minimize the maximum errors. Camera A's largest error is $6.8 \Delta E_{94}^*$. The errors form a tight grouping. As a comparison, the digitized film has errors up to $12 \Delta E_{94}^*$ and the grouping is broadly dispersed.

The differences in estimation accuracy between the ColorChecker and the artist paint target, underscores the importance of independent verification. Achieving high estimation accuracy for a characterization target is much simpler than achieving high accuracy when using the system for imaging paintings.

As an estimation problem, residual errors result, the magnitude of the errors dependent on the inherent properties of the camera and also on the method of estimation. A linear method has been described; nonlinear methods may result in improved performance, shown in Ref. 6 or using higher order matrices or multi-dimensional look-up tables. This is an evolving area of research. However, no matter how complex the color management system, the trends described above would persist: Digitized photographic positive transparencies and densitometric-type scanbacks (Camera C) will always result in large estimation errors; the improvement in performance is correlated with the similarity of a input device's spectral sensitivities to the human visual system.

The above analyses lead to the following recommendations: The archival master image should be the raw data, converted to a standardized format such as 16-bit TIFF uncompressed. Ideally, the image should include the work of art, a gray scale, and a color target. The color target should replace the Kodak Separation Guide. Because the TIFF format supports image tags (TIFF stands for Tagged Image File Format), spectral data of the gray scale and color targets should be a part of the tag. If possible, the spectral power distribution of the illumination and the spectral sensitivities of the camera system should also be included. If it isn't practical to include characterization targets in the image, the average digital counts of each target's color patches, captured under identical conditions, should be included in

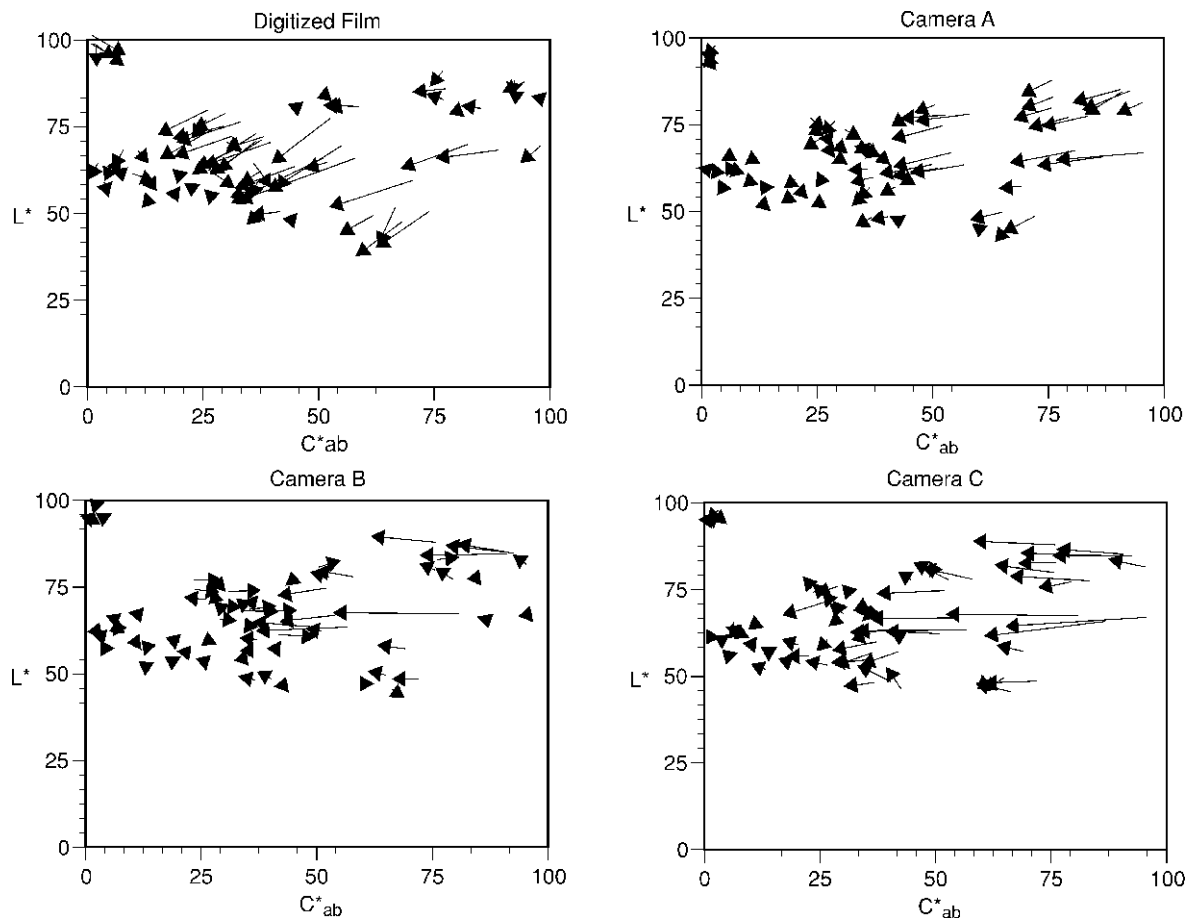


Figure 24. CIELAB $L^*C^*_{ab}$ projection vector plots showing estimation errors for the artist oil target.

the tag. A dictionary of standard image metadata is in preparation by the National Information Standards Organization, NISO.⁵² Images of the characterization targets should also be archived. If 8 bit data must be stored, gamma correction between 1.8 and 2.4 should first be applied. Color management should not be applied to the digital master. Rather, color management should be applied to various derivative images. The necessary information to implement reasonable color management stems from the characterization targets.

The Future

As color measurement developed during the 20th Century, there was a transition from predominantly colorimeters to predominantly spectrophotometers. That is, trichromatic instruments were replaced with spectral instruments. The principal advantages were numerous. The spectral data enabled an object's color to be calculated for any illuminant and observer of interest. Thus, the quality of a color match could be evaluated under any number of illuminating and viewing conditions. Second, the spectral data enabled a variety of analytical analyses such as colorant identification, instrumental-based color matching, and colorant strength.⁶ Finally, and perhaps most importantly, the presence or absence of metamerism could be readily observed. As an illustrative example, Pablo Picasso's *The Tragedy* was restored in 1937 and 1997. During 1937, paint losses were filled and inpainted. See the National Gallery of Art

website: www.nga.gov. The inpainted areas appear purplish when photographed, easily seen in the bottom-right portion of the web image. Spectral measurements of untreated and inpainted areas reveal that Picasso used prussian blue while the conservator used ultramarine blue, shown in Fig. 26. Unfortunately, most of the 1937 inpainting could not be removed during 1997; hence the pigment mismatch persists. Because the spectral sensitivity of the red sensitive layer of film is shifted towards longer wavelengths compared with the human visual system as shown in Fig. 9, the ultramarine was reproduced as a grayish purple rather than a grayish blue. Spectral measurements would have alerted the conservator that a metameric match was produced. This specific problem with blue pigments has been described by Staniforth.⁵³ Clearly, an imaging spectrometer would be a useful analytical tool. Furthermore, the lack of colorimetric accuracy, causing the large color shift in this example, and the need to standardize an illuminant and observer, as described above, would be eliminated.

Spectral-based imaging of artwork is currently at a research stage, summarized in Refs. 49 through 51. Using camera A, a novel approach to spectral imaging was evaluated in which a second image, taken by filtering the camera lens with a light blue filter (Wratten 38), was combined computationally to estimate the spectral reflectance of an image area.⁵⁴⁻⁵⁷ The spectral and camera data of the Kodak Gray Scale and ColorChecker chart were used to derive the necessary transforms. Following spectral estimation, CIELAB coordinates

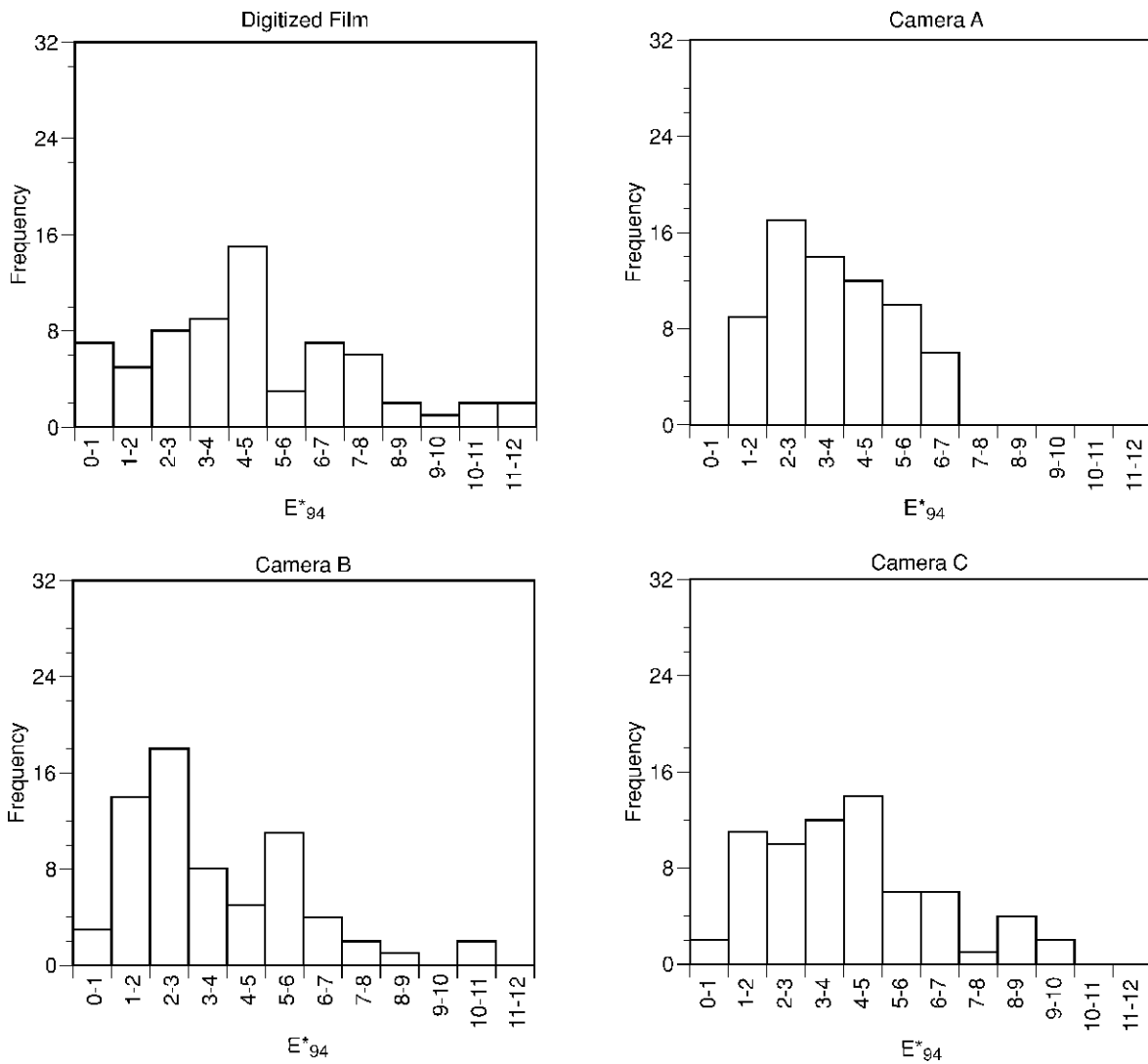


Figure 25. CIE94 color difference histogram showing estimation errors for the artist oil target

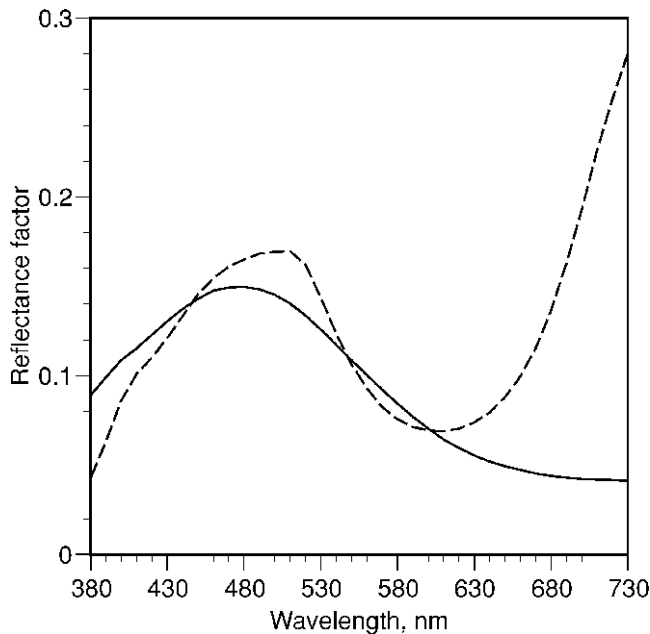


Figure 26. Spectral reflectance factor measurements of Pablo Picasso's *The Tragedy* (solid line) and 1937 inpainting (dashed line).

were calculated in the usual way. The ColorChecker was estimated to an average accuracy of $0.3\Delta E^*_{94}$ ($1.6\Delta E^*_{ab}$). The artist's paint target had an average accuracy of $2.0\Delta E^*_{94}$, nearly a twofold improvement in colorimetric accuracy.

One of the very interesting aspects of this spectral estimation approach is that spectra are generated from a conventional digital color camera. The spectra can be used for a variety of color reproduction⁵⁸⁻⁶¹ and conservation⁶²⁻⁶⁵ applications. Using only spectral information from the ColorChecker chart, the estimated spectral reflectance factor data for four blue pigments from the artist's paint target are plotted in Fig. 27. The fits are fairly typical of spectral-estimation techniques: the estimates tend to have greater spectral selectivity. The overall shapes are reasonably predicted. These estimated spectra were evaluated using a statistical method of pigment identification based on reflectance spectrophotometry.⁶⁵ The following pigments formed the database of possible blue pigments: cobalt, ultramarine, manganese, prussian, phthalocyanine, cerulean, and indanthrone. The database was formed from the artist's paint target. The cobalt and ultramarine blue spectra were correctly identified. Manganese blue was incorrectly identified as phthalocyanine

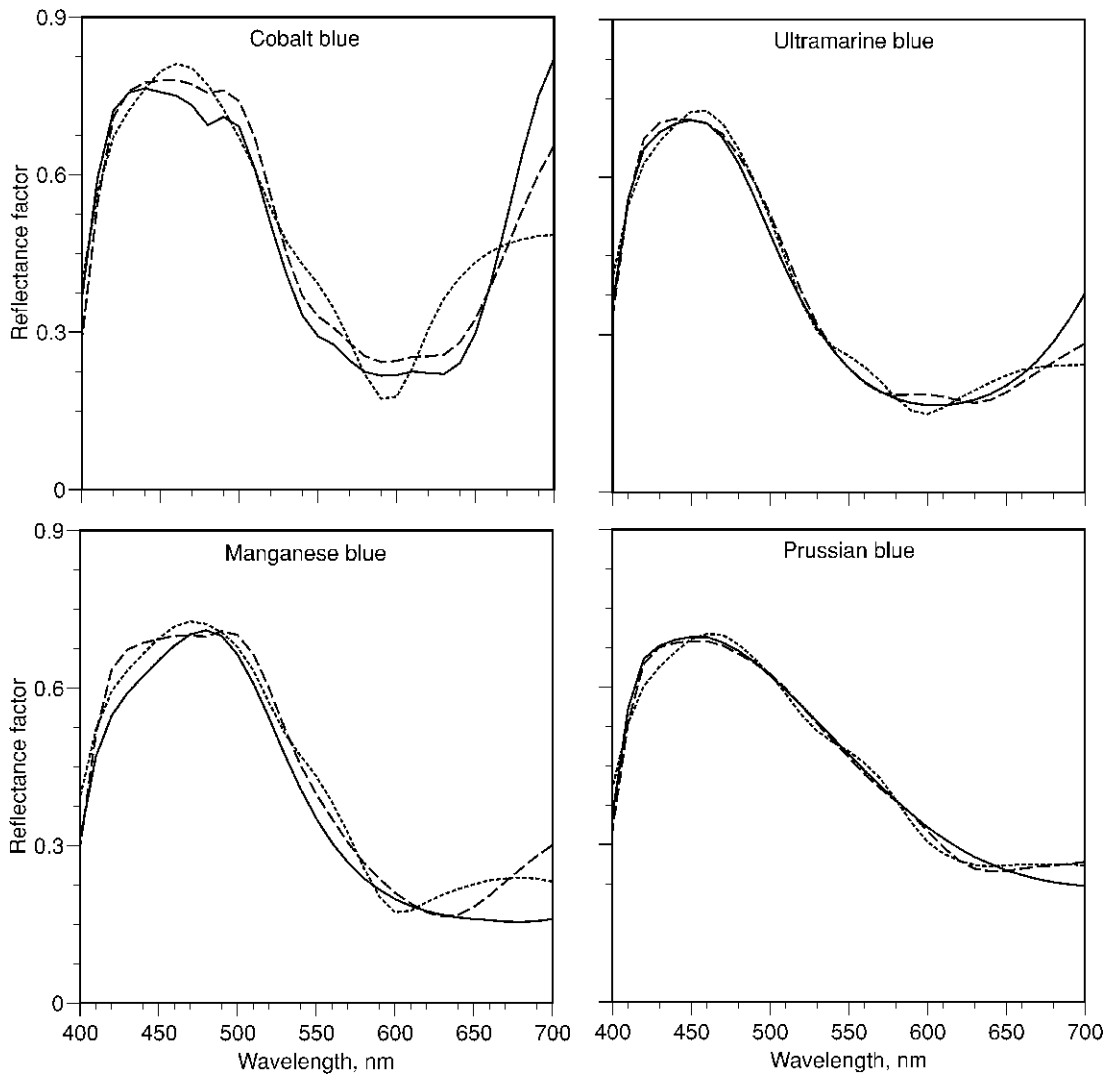


Figure 27. Spectral estimation of four samples from the artist oil target shown in Fig. 23: measured, solid line, estimated from spectral data of ColorChecker, dotted line, estimated from spectral data of the entire target, dashed line.

blue. This was due to the secondary peak at 650 nm in the estimated spectrum. The prussian blue sample was incorrectly identified as manganese blue. The spectral estimation was repeated, except that spectral information from the entire painted target was used in place of the ColorChecker. The estimated spectra are also plotted in Fig. 27. In all cases the spectral fits are improved. The pigment identification was repeated. Only the prussian blue sample was incorrectly identified, again as manganese blue. Given the known similarity in spectral properties between prussian and manganese blues,⁵³ these results were very encouraging.

Conclusions

An archival digital image of a work of art should facilitate a variety of applications including web-based images, color reproduction, scientific study, art historical and other scholarly studies, and most importantly, an accurate recording of its physical properties. As described, achieving an accurate recording is difficult and requires specialized hardware, optimal imaging practices, and specialized software.

Two issues need to be emphasized. The first is that scanback sensors are very common among the museum community. Because the number of pixels is often the dominant criterion when specifying an imaging system, scanbacks fare quite well. However, the majority of tri-filter scanbacks are densitometric rather than colorimetric. As described above, this results in very poor color accuracy, even following color management. There are two solutions: redesign the filter array, e.g., Ref. 66, or use a monochrome sensor and filter-wheel assembly with appropriate filter spectral transmittances. In general, greater emphasis needs to be placed on a sensor's spectral sensitivities. For accurate color imaging, sensors need to be closely related to the human visual system. This aspect of camera design is often overlooked. For example, Koelling⁶⁷ listed the five most important technical issues for digitizing works of art as image resolution, file format, file storage, file refreshment, i.e., updating storage media, and copyright. Hernandez⁶⁸ defined key digital camera selection criteria as dynamic range, optical resolution, bit depth, scanning area, and software.

The second issue to be emphasized is that image editing visual techniques to improve color accuracy has not

been included in this article. This was deliberate and not an omission. Visual matching between objects and their CRT representation is very complex and is highly dependent on viewing conditions,^{26,41} cognitive aspects given the dissimilar nature of light-emitting and light-reflecting stimuli,⁴¹ the observer,^{7,8} and monitor calibration.^{23–25} Any display will be highly metameric to reflective works of art. Furthermore, color management must be used, an evolving area of color technology.^{6,15,32} Transforming the raw camera signals to a derivative image such as an sRGB image should be a computational exercise, not a visual adjustment. The calculations are straightforward (a numerical example is given in Ref. 6) and eliminate the natural tendency to boost contrast and color saturation caused by unmatched viewing conditions and color gamut limitations of CRT displays.

For those engaged or soon to be engaged in creating a digital archive, the recommendations described above should be seriously considered. At the very least, standardized (actual or *de facto*) gray scale and color targets must be included in each image. The image metadata or image tag must contain information about the targets and details of the image-capture system. ▲

Acknowledgment. This publication was written while the author was a Senior Fellow in Conservation Science at the National Gallery of Art, Washington; the Gallery's financial support is sincerely appreciated. The author gratefully acknowledges the assistance of Janet Bliburg, Lorene Emerson, and Lyle Peterzell in collecting digital and conventional images, and Ross Merrill in producing the artist oil paint chart, all of the National Gallery of Art, Washington. Finally, the following imaging professionals were very helpful in reviewing manuscripts and providing the benefits of their extensive experiences: Franziska Frey, Image Permanence Institute; Connie McCabe, National Gallery of Art; Edward Giorgianni, Eastman Kodak Company; Mike Collette, Better Light; John Stokes, Stokes Imaging; Michael Stokes, Microsoft Corporation; and Francisco Imai, Munsell Color Science Laboratory. Francisco Imai also performed the spectral estimations.

References

1. S. Chapman, Guidelines for image capture, Research Libraries Group, www.rlf.org/preserv/joint/chapman.html (1998).
2. F. S. Frey and J. M. Reilly, *Digital Imaging for Photographic Collections: Foundations for Technical Standards*, Image Permanence Institute, Rochester Institute of Technology, Rochester, New York, 1999.
3. Guides to quality in visual resource imaging, Research Libraries Group, www.rlg.org/visguides/index.html (2000).
4. B. Blackwell, Light exposure to sensitive artworks during digital photography, *Spectra* **26**(2), 24–28 (2000).
5. N. Lossau and M. Liebethuth, Conservation issues in digital imaging, *Spectra* **26**(2), 30–36 (2000).
6. R. S. Berns, *Billmeyer and Saltzman's Principles of Color Technology*, 3rd ed., John Wiley & Sons, New York, 2000.
7. B. A. Wandell, *Foundations of Vision*, Sinauer Assoc. Inc., Sunderland MA, 1995.
8. P. K. Kaiser and R. M. Boynton, *Human Color Vision*, 2nd ed., Optical Society of America, Washington, DC, 1996.
9. A. Stockman, D. I. A. MacLeod and N. E. Johnson, Spectral sensitivities of the human cones, *J. Opt. Soc. Am. A* **10**, 2491–2521 (1993).
10. ISO/IEC DIS 10918-4, Information technology—Digital compression and coding of continuous-tone still images: Registration of JPEG profiles, SPIFF profiles SPIFF tags, SPIFF colour spaces, APPN markers, SPIFF compression types and Registration Authorities (REGAUT), International Organization for Standardization, Geneva, Switzerland.
11. CIE No. 15.2, Colorimetry, 2nd ed., Commission Internationale de l'Éclairage, Vienna, Austria, 1986.
12. D. S. Falk, D. R. Brill and D. G. Stork, *Seeing the Light: Optics in Nature, Photography, Color, Vision, and Holography*, John Wiley &

13. G. Holst, *CCD Arrays, Cameras, and Displays*, 2nd ed, SPIE, Intl. Soc. For Optical Eng., Bellingham, WA, 1998.
14. H. E. Ives, The transformation of color-mixture equations from one system to another, *J. Franklin Inst.* **180**, 673–701 (1915). Reproduced in D. L. MacAdam, Ed., *Selected Papers on Colorimetry – Fundamentals*, SPIE Milestone Series, Vol. MS 77, SPIE, Intl. Soc. For Optical Eng., Bellingham WA, 1993, pp. 57–71.
15. E. J. Giorgianni and T. E. Madden, *Digital Color Management Encoding Solutions*, Addison Wesley, Reading, MA, 1998.
16. F. Frey and R. Gschwind, Mathematical bleaching models for photographic three-color materials, *J. Imag. Sci. Technol.* **38**, 513–519 (1994).
17. R. Gschwind and F. Frey, Electronic imaging, a tool for the reconstruction of faded color photographs, *J. Imag. Sci. Technol.* **38**, 520–525 (1994).
18. R. S. Berns and M. J. Shyu, Colorimetric characterization of a desktop drum scanner using a spectral model, *J. Electronic Imag.* **4**, 360–372 (1995).
19. http://www.pima.net/standards/iso/tc42/wg18/kp_sfr_measure.htm from the Photographic and Imaging Manufacturing Association.
20. C. D. Child, Discharge from hot CaO, *Phys. Rev.* **32**, 492–511 (1911).
21. I. Langmuir, The effect of space charge and residual gases on thermionic current in high vacuum, *Phys. Rev.* **2**, 450–486 (1913).
22. T. H. James and G. C. Higgins, *Fundamentals of Photographic Theory*, Morgan & Morgan Inc., Hastings-on-Hudson, NY, 1968.
23. IEC 61966-2-1, Colour measurement and management in multimedia systems and equipment—Part 2-1: Colour management—Default RGB colour space—sRGB, International Electrotechnical Commission, Geneva, Switzerland, 1999.
24. R. S. Berns and N. Katoh, The digital to radiometric transfer function for computer controlled CRT displays, *Proc. CIE Expert Symposium '97 Colour Standards for Image Technology*, Commission Internationale de l'Éclairage, Vienna, Austria, 1997, pp 34–37, 1997.
25. T. Deguchi, N. Katoh and R. S. Berns, Clarification of 'gamma' and the accurate characterization of CRT monitors, *Proc. SID* **30**, 786–789 (1999).
26. R. W. G. Hunt, *The Reproduction of Colour in Photography, Printing, and Television*, 5th ed., Fountain Press, England, 1995.
27. ISO 14524, Photography—Electronic still picture cameras—Methods for measuring opto-electronic conversion functions (OECFs), International Organization for Standardization, Geneva, Switzerland. See also http://www.pima.net/standards/iso/tc42/wg18/WG18_POW.htm#14524.
28. ISO 12641, Graphic technology — Prepress digital data exchange — Colour targets for input scanner calibration, International Organization for Standardization, Geneva, Switzerland. (Commonly known as ANSI IT8.7/1 and 7/2.)
29. ISO 12642 Graphic technology – prepress digital data exchange – input data for characterization of 4-colour process printing, International Organization for Standardization, Geneva, Switzerland. (Commonly known as ANSI IT8.7/3.)
30. C. S. McCamy, H. Marcus and J. G. Davidson, A color-rendition chart, *J. Appl. Phot. Eng.* **2**, 95–99 (1976).
31. ISO 13655, Graphic technology—Spectral measurement and colorimetric computation for graphic arts images, International Organization for Standardization, Geneva, Switzerland.
32. ICC.1: 1998-09, File format for color profiles International Color Consortium, and ICC.1A: 1999-04, 'Addendum 2 to Spec. ICC.1:1998-09,' www.color.org (1999).
33. CIE No. 116, Industrial colour-difference evaluation, Commission Internationale de l'Éclairage, Vienna, Austria, 1995.
34. M. Stokes, M. D. Fairchild and R. S. Berns, Colorimetrically quantified tolerances for pictorial images, *TAGA part 2*, 757–778 (1992).
35. T. Song and R. Luo, Testing color-difference formulae on complex images using a CRT monitor, *Proc. 8th IS&T/SID Color Imaging Conference*, IS&T, Springfield, VA, 2000, pp 44–48.
36. ISO 15739, Photography—Electronic still picture cameras—Noise measurements, International Organization for Standardization, Geneva, Switzerland.
37. P. D. Burns and R. S. Berns, Image noise and colorimetric precision in multispectral image capture, *Proc. 6th IS&T/SID Color Imaging Conference*, IS&T, Springfield, VA, 1998, pp 83–85.
38. P. D. Burns and R. S. Berns, Quantization in multispectral color image acquisition, *Proc. 7th IS&T/SID Color Imaging Conference*, IS&T, Springfield, VA, 1999, pp 32–35.
39. T. Olson, Smooth ramps: Walking the straight and narrow path through color space, *Proc. 7th IS&T/SID Color Imaging Conference*, IS&T, Springfield, VA, 1999, pp 57–64.
40. B. Hill, T. Roger and F. W. Vorhagen, Comparative analysis of the quantization of color spaces on the basis of the CIELAB color-difference formula, *ACM Trans. Graphics* **16**, 109–154 (1997).
41. M. D. Fairchild, *Color Appearance Models*, Addison-Wesley, Reading, MA, 1998.
42. S. Publa and B. Roginski, NARA guidelines for digitizing archival materials for electronic access, National Archives and Records Administration, New York, 1986.

- tration, College Park, MD (1998). See also <http://www.nara.gov/nara/vision/eap/eapspec.html>.
43. F. C. Mintzer, L. E. Boyle, A. N. Cazes, B. S. Christian, S. C. Cox, F. P. Giordano, H. M. Gladney, J. C. Lee, M. L. Kelmanson, A. C. Lirani, K. A. Magerlein, A. M. B. Pavani, and F. Schiattarella, Towards on-line worldwide access to Vatican library materials, *IBM J. Research and Development*, **40**, 139–162 (1996). Also available at <http://www.almaden.ibm.com/journal/rd/mintz/mintzer.html>.
 44. F. Mintzer, Developing Digital Libraries of Cultural Content for Internet Access, *IEEE Communications* **37**(1), 72–78 (1999).
 45. F. P. Giordano, G. W. Braudaway, J. Christensen, J. Lee, and F. Mintzer, Evolution of a high-quality digital imaging system, *Proc. SPIE* **3650**, 110–118 (1999).
 46. K. Martinez, J. Cupitt and D. Saunders, High resolution colorimetric imaging of paintings, *Proc. SPIE* **1901**, 25–36 (1993).
 47. D. Saunders and J. Cupitt, Image processing at the National Gallery: The VASARI projec, *National Gallery Tech. Bull.* **14**, 72–86 (1993).
 48. A. Burmester, L. Raffelt, G. Robinson, and S. Wagini, The MARC project: From analogue to digital reproduction, in A. Burmester, L. Raffelt, K. Renger, G. Robinson, and S. Wagini, *Flämische Barockmalerei: Meisterwerke der Alten Pinakothek München; Flemish Baroque Painting: Masterpieces of the Alte Pinakothek München*, Hirmer Verlag, München, 1996, pp. 19–26.
 49. L. MacDonald and M. R. Luo, Eds., *Colour Imaging: Vision and Technology*, John Wiley & Sons, Chichester, 1999.
 50. *Proc. Intl. Symp. Multispectral Imaging and Color Reproduction for Digital Archives*, Chiba University, Soc. Multispectral Imaging Japan, 1999.
 51. *Proc. Second Intl. Symp. Multispectral Imaging and Color Reproduction for Digital Archives*, Chiba University, Soc. Multispectral Imaging Japan, 2000.
 52. See <http://www.niso.org/PR/Imagemeta.html>.
 53. S. Staniforth, Retouching and colour matching: The restorer and metamerism, *Studies in Conservation* **30**, 101–111 (1985).
 54. F. H. Imai and R. S. Berns, High-resolution multi-spectral image archives—A hybrid approach, *Proceedings IS&T/SID Sixth Color Imaging Conference*, IS&T, Springfield, VA, 1998, pp 224–227.
 55. R. S. Berns and F. H. Imai, Spectral estimation using trichromatic digital cameras, *Proc. Intl. Sym. Multispectral Imaging and Color Reproduction for Digital Archives*, Soc. Multispectral Imaging Japan, Chiba University, 1999, pp 42–49.
 56. F. H. Imai and R. S. Berns, A comparative analysis of spectral reflectance reconstruction in various spaces using a trichromatic camera system, *Proc. IS&T/SID Seventh Color Imaging Conference*, IS&T, Springfield, VA, 1999, pp 21–25.
 57. F. H. Imai, M. R. Rosen and R. S. Berns, Comparison of spectrally narrow-band capture versus wide-band with a priori sample analysis for spectral reflectance estimation, *Proc. 8th IS&T/SID Color Imaging Conference*, IS&T, Springfield, VA, 2000, pp 234–241.
 58. R. S. Berns, Challenges for colour science in multimedia imaging systems, in L. MacDonald, and M.R. Luo, Eds., *Colour Imaging: Vision and Technology*, John Wiley & Sons, England, 1999, pp. 99–127.
 59. R. S. Berns, F. H. Imai, P. D. Burns, and D. Y. Tzeng, Multi-spectral-based color reproduction research at the Munsell Color Science Laboratory, *Proc. SPIE* **3409**, 14–25 (1999).
 60. F. H. Imai, M. R. Rosen, R. S. Berns, and D. Tzeng, Spectral reproduction from scene to hardcopy I: Image input and output, *Proc. SPIE*, in press (2001).
 61. M. Rosen, F. Imai, X. Jiang, and N. Ohta, Spectral reproduction from scene to hardcopy II: Image processing, *Proc. SPIE*, in press (2001).
 62. S. Baronti, A. Casini, F. Lotti, and S. Porcinai, A multispectral imaging system for mapping of pigments in works of art by the use of principal-component analysis, *Appl. Optics* **37** 1299–1309 (1998).
 63. A. Casini, F. Lotti, M. Picollo, L. Stefani, and E. Buzzegoli, Image spectroscopy mapping technique for non-invasive analysis of paintings, *Studies in Conservation* **44** 39–48 (1999).
 64. J. Thoma, J. Cupitt and D. Saunders, An investigation of the potential use of visible-region multispectral imaging for pigment identification in paintings, *Proc. Colour Image Science 2000*, Colour and Imaging Institute, University of Derby, Derby, UK, 2000, pp 95–106.
 65. R. S. Berns, J. Krueger and M. Swicklik, Multiple pigment selection for inpainting using visible reflectance spectrophotometry, *Studies in Conservation*, in press 2001.
 66. S. Quan, N. Ohta and N. Katoh, Optimization of camera spectral sensitivities, *Proc. 8th IS&T/SID Color Imaging Conference*, IS&T, Springfield, VA, 2000, pp 273–278.
 67. J. M. Koelling, Revealing history – digital imaging, the new photographic research tool, *Spectra* **26**(2), 10–15 (2000).
 68. C. Hernandez and R. Lilien, Building a digital archive – digitizing for the long term, *Spectra* **26**(2), 16–17 (2000).